haematologica
Journal of The Ferrata Storti Foundation

An intronic deletion in megakaryoblastic leukemia 1 is associated with hyperproliferation of B cells in triplets with Hodgkin lymphoma

by Julien Record, Anton Sendel, Joanna S. Kritikou, Nikolai V. Kuznetsov, Hanna Brauner, Minghui He, Noemi Nagy, Mariana M.S. Oliveira, Elena Griseti, Christoph B. Haase, Jenny Dahlström, Sanjaykumar Boddul, Fredrik Wermeling, Adrian J. Thrasher, Chaohong Liu, John Andersson, Hans-Erik Claesson, Ola Winqvist, Siobhan O. Burns, Magnus Björkholm, and Lisa S. Westerberg

Haematologica 2019 [Epub ahead of print]

Citation: Julien Record, Anton Sendel, Joanna S. Kritikou, Nikolai V. Kuznetsov, Hanna Brauner, Minghui He, Noemi Nagy, Mariana M.S. Oliveira, Elena Griseti, Christoph B. Haase, Jenny Dahlström, Sanjaykumar Boddul, Fredrik Wermeling, Adrian J. Thrasher, Chaohong Liu, John Andersson, Hans-Erik Claesson, Ola Winqvist, Siobhan O. Burns, Magnus Björkholm, and Lisa S. Westerberg. An intronic deletion in megakaryoblastic leukemia 1 is associated with hyperproliferation of B cells in triplets with Hodgkin lymphoma.
Haematologica. 2019; 104:xxx
doi:10.3324/haematol.2019.216317

An intronic deletion in megakaryoblastic leukemia 1 is associated with hyperproliferation of B cells in triplets with Hodgkin lymphoma

Julien Record[1*], Anton Sendel[1*], Joanna S. Kritikou[1], Nikolai V. Kuznetsov[1], Hanna Brauner[1], Minghui He[1], Noemi Nagy[1], Mariana M.S. Oliveira[1], Elena Griseti[1], Christoph B. Haase[1], Jenny Dahlström[2], Sanjaykumar Boddul[2], Fredrik Wermeling[2], Adrian J. Thrasher[3], Chaohong Liu[4], John Andersson[1,5], Hans-Erik Claesson[2], Ola Winqvist[2], Siobhan O. Burns[6,7], Magnus Björkholm[2], Lisa S. Westerberg[1]

[1]Department of Microbiology Tumor and Cell Biology, Biomedicum, Karolinska Institutet, Stockholm, Sweden; [2]Department of Medicine Solna, Karolinska University Hospital, Stockholm, Sweden; [3]Institute of Child Health, University College London, London, United Kingdom; [4]Department of Pathogen Biology, School of Basic Medicine, Huazhong University of Science and Technology, Wuhan, China; [5]Department of Medical Epidemiology and Biostatistics, Karolinska Institutet, Stockholm, Sweden; [6]Institute of Immunity and Transplantation, University College London, London, United Kingdom; [7]Department of Immunology, Royal Free London NHS Foundation Trust, London, United Kingdom

* J.R. and A.S. contributed equally to this work

Corresponding author:

Lisa Westerberg, PhD, Associate Professor, Department of Microbiology, Tumor and Cell Biology; Karolinska Institutet, Biomedicum, Solnavägen 9, SE-171 77 Stockholm, Sweden, Phone: +46 8 524 86833; Fax: +46 8 524 87150; E-mail: lisa.westerberg@ki.se

Short title: Intronic deletion in *MKL1* alters B cell function

Abstract: 239 words

Full text: 4042 words

Figures: 6 figures

Supplemental information: 1 table and 9 supplemental figures

Reference count: 50

Keywords: Megakaryoblastic leukemia 1 (MKL1), Hodgkin lymphoma (HL), B cells, actin cytoskeleton

Key points

- An intronic deletion in *MKL1* leads to increased MKL1 activity and actin content in B cells
- Increased MKL1 activity leads to B cell hyperproliferation, genomic instability, and increased tumor growth

Abstract

Megakaryoblastic leukemia 1 (MKL1) is a coactivator of serum response factor and together regulate transcription of actin cytoskeleton genes. MKL1 is associated with hematologic malignancies and immunodeficiency, but its role in B cells is unexplored. Here we examined B cells from monozygotic triplets with an intronic deletion in *MKL1*, two of whom were previously treated for Hodgkin lymphoma. To investigate MKL1 and B cell responses in HL pathogenesis, we generated Epstein Barr virus-transformed lymphoblastoid cell lines from the triplets and two controls. While cells from the Hodgkin lymphoma treated patients had a phenotype close to healthy controls, cells from the undiagnosed triplet had increased *MKL1* mRNA, increased MKL1 protein, and elevated expression of MKL1-dependent genes. This was associated with elevated actin content, increased cell spreading, decreased expression of CD11a integrin molecules, and delayed aggregation. Moreover, cells from the undiagnosed triplet proliferated faster, displayed a higher proportion of cells with hyperploidy, and formed large tumors *in vivo*. This phenotype was reversible by inhibiting MKL1 activity. Interestingly, cells from the triplet treated for Hodgkin lymphoma in 1985 contained two subpopulations: one with high expression of CD11a that behaved like control cells and the other with low expression of CD11a that formed large tumors *in vivo* similar to cells from the undiagnosed triplet. This implies that pre-malignant cells had re-emerged a long time after treatment. Together, these data suggest that dysregulated MKL1 activity participates in B cell transformation and Hodgkin lymphoma pathogenesis.

Introduction

Hodgkin lymphoma (HL) is a B cell malignancy of largely unknown etiology. Familial clustering and twin concordance is seen, as well as links to viral infections such as Epstein-Barr virus (EBV) (1, 2). The malignant HL Reed-Sternberg cells have frequently undergone class switch recombination and likely originate from germinal center B cells that fail to undergo apoptosis despite destructive somatic mutations (1, 3, 4). A number of studies have shown the ability of EBV to rescue crippled germinal center B cells from apoptosis, supporting its role in HL pathogenesis (5, 6).

Megakaryoblastic leukemia 1 (MKL1; also known as MRTF-A, MAL, or BSAC) is a transcriptional coactivator of serum response factor (SRF) and binds to globular (G-)actin via an RPEL motif (7, 8). As cytoplasmic G-actin is polymerized into filamentous (F)-actin, the G-actin pool diminishes. This leads to MKL1 translocation into the nucleus where it interacts with SRF to induce transcription of cytoskeleton-related genes, including actin, integrin molecules, and SRF itself (7-10). Indeed, inducible expression of SRF in response to serum stimulation is dependent on SRF and MKL1 activity (9, 11). Actin polymerization and MKL1-SRF activity are additionally regulated by extracellular signaling through several integrin molecules which activate the small Rho GTPases, including RhoA (12).

MKL1 was initially described as part of a fusion protein in megakaryoblastic leukemia of poor prognosis (13, 14). MKL1 expression is detected in malignant cells in breast and liver cancer and associated with increased cell proliferation, anchorage-independent cell growth, and metastasis (15, 16). Small molecule inhibitors of the MKL1-SRF pathway have been identified, facilitating studies on the biological activity of MKL1 and are tested as potential cancer therapeutic agents (17). One of these compounds is CCG-1423 that was originally identified as a RhoA-MKL1-SRF pathway inhibitor and later defined to directly target MKL1 (17, 18).

A loss-of-function mutation in *MKL1* was recently identified in a 4-year-old girl with severe primary immunodeficiency (19). MKL1 deficiency caused reduced G-actin and F-actin content in patient neutrophils leading to reduced phagocytosis and migration (19). In 2013, a familial case of two monozygotic triplets that developed HL at the age of 40 and 63 was described (20). Both patients are in remission upon HL treatment in 1985 and 2008 and the third triplet remains undiagnosed. Using microarray comparative genomic hybridization, a 15–31-kb deletion in intron 1 of *MKL1* was identified in the triplets (20). The impact of this mutation on MKL1 expression and B cell function remains unknown.

We here took the approach to generate EBV-transformed lymphoblastoid cell lines (LCLs) from the triplets with the deletion in *MKL1* intron 1 (HL0, HL1, and HL2) and two healthy controls (C1 and C2). We found that the LCLs from the undiagnosed triplet had increased MKL1 and SRF expression, and elevated G-actin content. This was associated with hyperproliferation, genomic instability, and tumor formation when injected into immunocompromised mice. When compared to control LCLs with high CD11a expression and capacity to form large aggregates, HL0 LCLs expressed low CD11a and had reduced capacity to form aggregates. The HL1 LCLs showed a bimodal expression of CD11a and when sorted for CD11a low and CD11a high cells, CD11a high cells mimicked the response of control LCLs whereas HL1 CD11a low cells mimicked the response of HL0 cells with increased proliferation and tumor formation. Finally, treatment of HL0 cells with the MKL1 inhibitor CCG-1423 reverted the phenotype and prevented tumor growth *in vivo*. This data shows that unregulated MKL1 alters B cell cytoskeletal responses leading to B cell transformation.

Methods

Human blood samples and EBV transformation

Whole blood samples were obtained from the triplets and age-matched controls after informed consent was given. This study was performed according to the principles expressed in the Helsinki Declaration and with approval from the local ethics committee (Dnr 2015/416-31). For analysis of primary cells, the first experiment included samples from HL0, HL1, and ctrl (not used for EBV-transformation) collected in February 2015 and the second experiment HL2 and C1, collected in May 2015. To establish EBV-transformed LCLs, PBMCs from HL0, HL1, and HL2, and two age- and sex-matched controls (C1 and C2), all collected in November 2015, were cultured with supernatant of the virus-producing B95-8 line (21).

Mice

NOD/SCID-IL2rγ^{null} (NSG) mice were bred and maintained at the animal facility of the Department of Microbiology, Tumor and Cell Biology at Karolinska Institutet under specific pathogen-free conditions. Female mice were used and all animal experiments were performed after approval from the local ethics committee (the Stockholm District Court, permit N77/13 and N272/14). For inhibitor treatment, 10 μM CCG-1423 or DMSO was injected intratumorally for 6 consecutive days. The volume of the tumor was calculated at the endpoint using a caliper.

Flow cytometry and Microscopy

Flow cytometry was performed on PBMCs, LCLs, and cultured primary B cells using the LSRFortessa X-20 (BD Biosciences) and results were processed using FlowJo v10 software (TreeStar Inc., St. Ashland, Oregon, USA). To determine integrin expression at the cell surface, LCLs were labeled with an anti-human CD11a antibody (TS2/4; Biolegend) for total CD11a expression, or an anti-human CD11a antibody (Hl111; Biolegend) for inactive/closed conformation-CD11a expression, or an anti-human CD54 antibody (Biolegend), followed by an anti-mouse-

Alexa647 antibody (ThermoFisher Scientific). To determine F- and G-actin content in two LCL samples side by side, one sample was incubated with an anti-human CD54 antibody (Biolegend) for 30 minutes on ice and thereafter labeled with DNaseI-Alexa488 (ThermoFisher Scientific) and phalloidin-Alexa568 (ThermoFisher Scientific).

Results

The *MKL1* intron 1 deletion is associated with increased expression of MKL1 and MKL1-induced genes.

To understand how the deletion in *MKL1* intron 1 affected actin cytoskeleton regulation in B cells, we examined freshly isolated cells and LCLs from the triplets (HL0, HL1, and HL2) and two healthy controls (C1 and C2; Figure 1A-B). We reasoned that the undiagnosed HL0 triplet may represent the pre-HL stage, whereas HL1 and HL2 cells may be more similar to control cells because of successful treatment for HL in 1985 and 2008, respectively. MKL1 protein in primary blood lymphocytes was higher in all triplets when compared to control cells as assessed by flow cytometry (Figure 1C and S1A). Using primer walking and sequencing, we confirmed that the triplets contained a heterozygous deletion of *MKL1* intron 1 (Figure S2A). The intron 1 is in the 5´ untranslated region of the *MKL1* gene. We examined exon boundaries of exon 1-4 in the 5' untranslated region and found normal expression of adjacent exons, suggesting that the intron 1 deletion did not affect splicing of *MKL1* (Figure S3). *MKL1* intron 1 contains many transcription binding sites (Figure S2B) that may affect MKL1 transcription. We examined *MKL1* mRNA expression in LCLs by RT-qPCR. HL0 (undiagnosed triplet) LCLs had higher expression of *MKL1* when compared to the siblings (HL1 and HL2) and controls (C1 and C2) (Figure 1D). Detection of MKL1 protein indicated that HL0 LCLs displayed higher MKL1 than C1 and C2 (Figures 1E-F and S1B). To investigate whether increased MKL1 expression was associated with increased MKL1 activity, we examined mRNA expression of specific MKL1-dependent genes including *SRF* and *ACTB* (19). HL0 LCLs had the highest expression for both MKL1-dependent genes (Figure 1G).

This suggests that the intron 1 deletion in *MKL1* directly influences the expression of MKL1 and MKL1 target genes.

Increased actin content and actin-dependent spreading in HL0 and HL1 cells.

To understand how the deletion in *MKL1* intron 1 affected actin content and responses, we examined F-actin content in primary lymphocytes by flow cytometry. No difference was seen when comparing HL0 and HL1 to control lymphocytes while HL2 had higher F-actin content when compared to C1 (Figure 2A). In primary monocytes gated based on FSC and SSC profiles by flow cytometry, triplet cells had higher MKL1 expression (Figure S1C) and higher F-actin content (Figure S1D). Moreover, control and patients monocyte-derived dendritic cells from whole blood displayed a similar ability to form podosomes (Figure S4A and B). To exclude a possible effect of cell size and different hematopoietic cell subsets of primary cells, we compared actin content in triplet LCLs with controls side by side by alternately labelling one cell population with anti-CD54 antibodies after fixation and before mixing the two populations. We thereafter detected G-actin using DNAse1, and F-actin using phalloidin (Figure 2B and S1E-F). HL0 cells had increased G-actin and a tendency for increased F-actin (Figure 2B-D). To examine if increased actin content had any impact on cytoskeletal rearrangement, triplet and control LCLs were examined microscopically on glass surfaces coated with fibronectin and anti-CD19 antibodies. HL0 and HL1 cells had increased capacity to spread with formation of long dendritic protrusions (Figure 2E-F and S5A) and increased adhesive area measured by interference reflection microscopy (Figure 2G-H). This indicates that the deletion in *MKL1* intron 1 was associated with increased actin content and actin-dependent B cell spreading.

HL0 cells display decreased aggregation and reduced CD11a integrin expression.

LCLs grow in clusters by homotypic aggregation dependent on leukocyte function antigen-1 (consisting of subunits CD11a/integrin αL and CD18/integrin β2) and intercellular adhesion

molecule-1 (ICAM-1/CD54, Figure S6) (22-24). When culturing LCLs, we observed decreased clustering of triplet cells, especially pronounced for HL0 LCLs (Figure S5B). To quantify this, we measured aggregation from single cell suspensions by live cell imaging during 2 hours. C1, C2, HL1, and HL2 LCLs formed aggregates instantly, whereas HL0 LCLs displayed impaired aggregation with delayed formation of small aggregates over 2 hours (Figure 3A-B). We examined if decreased aggregation resulted from altered surface expression of adhesion receptors. C1, C2, HL1, and HL2 cells displayed similar expression of total surface and intracellular CD11a, and inactive CD11a (Figure 3C-G and S5C). HL0 cells displayed lower expression of total surface and intracellular CD11a, and inactive CD11a as well as lower CD11a mRNA (*ITGAL*, Figure 3C-G and S5C). Interestingly, cells lacking MKL1 expression (19) showed higher surface CD11a expression when compared to control cells (Figure S4C). Triplet and control LCLs had similar expression of CD54 (Figure 3H and S5C). This shows that HL0 cells had reduced capacity to form aggregates and this was associated with low expression of CD11a.

HL0 cells display increased proliferation and genomic instability.

HL has previously been associated with immunodeficiency and altered proliferation (25, 26). To examine for immunodeficiency, we used FASCIA (Flow-cytometric assay of specific cell-mediated immune response in activated whole blood) analysis to detect B and T cell responses to various antigens (27). We found that triplet B cells displayed a decreased response to pokeweed mitogen but had normal T cell responses (Table S1). To address how increased MKL1 expression correlated to proliferation, primary B cells were cultured with anti-CD40 antibodies and IL-4 for 72 hours and labelled with the proliferation marker Ki-67 (Figure 4A and S5D). Triplet samples had more Ki-67^{+} proliferating B cells than controls (Figure 4A). To exclude the variation due to sample collection time when using Ki67, we measured proliferation in LCLs by DNA syntesis over 20 hours using ^{3}H-thymidine incorporation. Compared to controls, HL0 cells had higher DNA synthesis (Figure 4B). To examine if proliferation rate was associated with cell cycle alterations, we used DNA-

specific Hoechst labeling to evaluate cells in G0/G1 (2n DNA content), S, and G2/M (4n DNA content) phases. The proportion of cells in S or G2/M phase was higher in HL0 LCLs (Figure 4C). 3% of HL0 cells had more than 4n DNA content, compared to 0–1% of control cells (Figure 4D). Since EBV has been shown to induce multiple nuclei in transformed cells (28), we counted nuclei in triplet and control LCLs to evaluate if multinuclearity could explain the proportion of cells with more than 4n DNA content. No correlation was seen between multinuclearity and DNA content (Figure 4E-F), indicating that increased DNA content could have resulted from genomic instability. When arresting triplet and control LCLs in metaphase, HL0 and HL1 had a higher proportion of cells (approximately 25–35 %) with more than 46 chromosomes (Figure 4G-H). To investigate the growth of HL0 and C1 cells *in vivo,* cells were injected subcutaneously into NSG mice that lack a functional immune response and cell growth was examined as tumor mass on day 9. C1 cells failed to form a tumor mass whereas HL0 cells formed tumors with distinct angiogenesis (Figure 4I). Together this suggests that increased MKL1 expression and activity is directly associated with hyperproliferation and genomic instability leading to formation of a tumor mass *in vivo.*

HL1 display two distinct populations of cells of which one shows an HL0 phenotype.

We noticed that HL1 cells recurrently showed an intermediate phenotype when compared to HL0 and control cells. HL1 cells showed a bimodal expression of CD11a and we examined if this represented two populations of cells with different phenotype. We used FACS sorting to sort out CD11a low and CD11a high cells from the HL1 cells (Figure 5A). Genomic DNA PCR showed that sorted HL1 CD11a low and HL1 CD11a high cells contained the heterozygous deletion of *MKL1* intron 1 (Figure S2A). CD11a low cells had increased MKL1 protein and increased cell spreading when compared to CD11a high cells (Figure 5B-C). We quantified aggregation during 2 hours and found that CD11a low cells had reduced capacity to aggregate when compared to CD11a high cells (Figure 5D-E). To examine proliferation, we sorted 250000 cells of CD11a low and CD11a high cells and counted cells at day 3–8. The CD11a high cells showed only modest proliferation whereas

the CD11a low cells expanded 3–4-fold during day 3–8 (Figure 5F). To examine proliferation of cells *in vivo*, we injected CD11a low and CD11a high cells into NSG mice and monitored tumor growth on day 15. CD11a low cells formed a large tumor mass with visible angiogenesis, whereas CD11a high cells formed a smaller tumor mass (Figure 5G). To address if the control C1 and C2 cells also contained a stable CD11a low population, we used FACS sorting and cultured the C1 and C2 CD11a low and CD11a high cells for 17 days. The C1 and C2 CD11a low cells gained expression of CD11a during the culture, suggesting that the CD11a phenotype in control cells was unstable (Figure S7-S8). We next examined if alterations in CD11a expression was found in the L1236 HL cell line derived from a primary isolate of a patient with advanced HL (29). The L1236 cells contained large Reed-Sternberg-like cells and smaller cells (Figure 5H). Using flow cytometry, small and large cells were identified based on FSC and SSC populations. Small cells had low expression of CD11a and the large cells were devoid of CD11a expression (Figure 5H). Together, this data suggests that low expression of CD11a may be a characteristic feature of pre-malignant B cells in HL.

Inhibition of MKL1 activity in HL0 cells induces a phenotype similar to control cells.

We next examined if we could revert the phenotype of HL0 cells to that of control cells using the MKL1 small molecule inhibitor CCG-1423 (17, 18). To define the dose range, HL0 cells were treated with different doses of CCG-1423 and cell death measured by flow cytometry. At 2–10 μM CCG-1423, 90% of cells were viable (Figure 6A). HL0 cells treated with CCG-1423 displayed dose-dependent lowering of MKL1 protein and decreased SRF expression (Figure 6B-D). The spreading capacity of HL0 cells was reduced upon CCG-1423 treatment (Figure 6E). Lowering MKL1 protein and activity led to increased aggregate formation and reduced proliferation (Figure 6F-H). To examine if the MKL1 inhibitor could suppress tumor growth *in vivo*, HL0 cells were injected into NSG mice by subcutaneous injections. At day 6–12, a daily dose of 10 μM CCG-1423

was injected intratumorally. When compared to mice treated with vehicle (DMSO), treatment with the MKL1 inhibitor led to reduced HL0 tumor mass (Figure 6I).

Discussion

Dysregulation of MKL1 expression and the actin cytoskeleton has been implicated in hematological malignancies, although the exact mechanism has not been determined (Figure S9) (30, 31). Mutated MKL1 was originally described in patients with acute megakaryoblastic leukemia where *MKL1* was fused with *RBM15* by a chromosomal translocation (13, 14). The role of MKL1 in megakaryocyte differentiation, migration, and in the formation of proplatelets was subsequently described in MKL1-deficient mice (32, 33). In humans, MKL1 deficiency greatly impacts the hematopoietic cell actin cytoskeleton resulting in severely impaired cell migration and phagocytosis (19). The genetically identical triplets with a large deletion in *MKL1* intron 1, HL affected and undiagnosed, provided a unique opportunity to investigate MKL1 and B cell responses in HL pathogenesis. We identify that increased activity of MKL1 in B cells led to the classical hallmarks of cancer cells: hyperproliferation, genomic instability, and formation of tumors with induction of angiogenesis (34).

We have in this study mainly used EBV-transformed B cells (LCLs) from two controls and the triplets. To minimize the possible variation due to EBV transformation, all samples were EBV-transformed under the same condition in regards to day of transduction, virus batch and concentration. The EBV cells allowed us to extensively investigate the impact of the *MKL1* intron 1 deletion on B cells and importantly perform controlled experiments where control and patient cells could be compared side by side. A limitation with EBV transformation is that highly proliferative B cells are favoured during EBV transformation (35). Moreover, the donor distribution of naïve, non-switched memory, and switched memory B cells are reflected in the EBV-transformed B cells (35, 36). We can not exclude that the EBV transformation induced expansion of a dominant subclone,

however, the CD11a staining revealed variable expression of CD11a in each sample although with different distribution. In fact, the variable CD11a expression allowed us to define different subpopulations in the HL0 and HL1 samples and argue against a dominant subclone upon EBV transformation.

Since the deletion in *MKL1* is intronic, we did not anticipate any changes in the amino acid sequence and found that MKL1 was expressed at normal size. The first intron is often essential for the regulation of gene expression (37, 38), why we investigated possible alterations of MKL1 expression in the triplet cells and found that cells from the undiagnosed triplet (HL0) displayed the highest expression of MKL1 while HL1 and HL2, the triplets who were successfully treated for HL, showed an intermediate phenotype. This suggests a phenotypical difference between the triplets based on the onset and treatment of the disease. MKL1 via its interaction with SRF regulates expression of hundreds of genes involved in cell migration, adhesion, and differentiation (15, 39). We show that the high mRNA and protein expression of MKL1 in HL0 cells correlated with high expression of MKL1 target genes *SRF* and *ACTB*. MKL1 activity promotes migration and proliferation of cancer cells (16, 40, 41), suggesting that HL0 LCLs could be pre-malignant.

Because the absence of MKL1 results in a severely impaired actin cytoskeleton (19), we reasoned that overexpression of MKL1 could result in a more active actin cytoskeleton. Actin cytoskeleton proteins are upregulated in invasive cancer (42), suggesting that the increased activity of the actin cytoskeleton in the HL0 cells could enhance cell migration and cell division, promoting invasion of cells and growth of tumors. In support of this, HL0 cells with the highest MKL1 expression had higher G- and F-actin content and displayed increased spreading, a process that depends on actin cytoskeleton dynamics. The migration and hyperproliferation of cancer cells are also regulated by the alteration of integrin expression at the cell surface and the modification of the subsequent intracellular integrin signaling (43). EBV-transformed B cells aggregate in cell culture via the

interaction between the integrin CD11a (subunit of LFA-1) and the adhesion molecule ICAM-1 (this study) (22-24). We examined LCL aggregation *in vitro* and observed that HL0 cells aggregated poorly, while HL1 cell aggregation varied and HL2 cell aggregation was similar to controls. We could show that the surface and total protein as well as the mRNA expression of CD11a was low in HL0 cells while similar to control in HL2 cells. Interestingly, CD11a expression in HL1 cells showed a bimodal distribution with CD11a low and CD11a high cells that might be the cause of the high variation of HL1 cell aggregation results. It is possible that the overactive actin cytoskeleton in HL0 cells prevented correct translocation of adhesion receptors to the cell surface or affected integrin inside-out and outside-in signalling.

Because of the possible pre-malignant stage of HL0 cells, we investigated the cell proliferation response *in vitro* and *in vivo* for formation of tumor mass. HL0 cells were hyperproliferative *in vitro* and also *in vivo* where HL0 cells rapidly formed tumors in immunocompromised NSG mice. The HL0 population showed increased DNA content and a higher percentage of hyperploid cells. Because polyploidy is a result of incomplete cytokinesis (44), the increased hyperploidy of HL0 cells could be due to an elevated rate of cytokinesis failure, possibly connected to overactivity of the actin cytoskeleton as shown previously when the actin regulator WASp is overactive (45, 46). Reed-Sternberg cells originate from failed cytokinesis and re-fusion of HL daughter cells (47, 48). This suggests that the failure of HL0 cells to complete cytokinesis could lead to the formation of giant multinucleated cells similar to Reed-Sternberg cells.

The variable phenotype of the HL1 and HL2 triplets treated for HL in 1985 and 2008, respectively, was at first puzzling. Since all triplets contained the heterozygous deletion of *MKL1* intron 1, we reasoned that whether a cell expresses the healthy *MKL1* allele or the intron 1 deleted allele of *MKL1* must be a stochastic event. The transcription of the *MKL1* gene is quite complex with several sets of transcripts. The transcriptional start site is in exon 4, placing intron 1 is in the 5’ untranslated

region of *MKL1*. To understand the MKL1 associated phenotype, we took advantage of the bimodal expression of CD11a in HL1 cells to sort out CD11a low and CD11a high cells. CD11a high cells behaved similar to the control cells, displaying low expression of MKL1, low spreading and proliferation, together with a strong aggregation response. In contrast, CD11a low cells behaved similar to HL0 cells with high expression of MKL1, decreased aggregation, as well as increased proliferation *in vitro* and tumor formation *in vivo*. We also sorted out the small population of CD11a low cells from the control C1 and C2 cells, however, control CD11a low cells were not stable in culture and started to express CD11a during 17 days of culture. This suggests that the stable CD11a low phenotype in HL0 cells and sorted HL1 cells is associated with increased MKL1 expression. Interestingly, HL Reed-Sternberg cells are characterized by low mRNA expression of CD11a (49, 50). Thus, since the HL0 triplet has not received HL treatment we reason that HL0 cells could represent a pre-HL stage. The presence of CD11a low cells in the HL1 patient, treated for HL using mustargen, oncovin, procarbazine, prednisone/adriamycin, bleomycin, vinblastine, and dacarbazine in 1985 (20), may indicate de novo HL with the CD11a low cells possibly outgrowing the healthy CD11a high cells. With this reasoning, the HL2 patient that received adriamycin, bleomycin, vinblastine and dacarbazine to treat HL in 2008 (20) would predominantly have CD11a high cells assuming that the highly proliferative CD11a low cells would have been mostly eradicated by the HL treatment.

Finally, we investigated if the HL0 cell phenotype could be reverted by inhibition of MKL1 using the small molecule CCG-1423 (17, 18). HL0 cells treated with the MKL1 inhibitor showed decreased expression of MKL1 protein and the MKL1 target gene *SRF*, as well as reduced cell spreading. Importantly, using the MKL1 inhibitor we could revert the hyperproliferation of HL0 cells *in vitro* and also by intratumoral injections *in vivo*.

We here present the first example of an intron mutation in *MKL1*, resulting in increased MKL1 expression, increased actin content, decreased aggregation, hyperproliferation, and genomic instability in B cells. Of the triplet samples, HL0 showed the most pronounced difference in both MKL1 expression and activity, as well as in cellular responses when compared to controls. HL1 and HL2 patient cells, successfully treated for HL, had a phenotype closer to healthy controls. This finding together with the known role of MKL1 in metastasis (15) and with high mRNA expression of MKL1 in many types of lymphomas, suggests that increased MKL1 expression actively participates in B cell transformation and HL pathogenesis.

Acknowledgements

We are grateful to the family and healthy controls for providing blood samples. We thank Dr Kaisa Lehti, Dr Peter Bergman, and Dr Andreas Lundqvist for valuable input. This work was supported by a postdoctoral fellowship from the Swedish Childhood Cancer Fund and from the Swedish Society of Medical Research to J.R., an MD-PhD (CSTP) fellowship and a clinical internship (research AT) from Karolinska Institutet to A.S., a clinical postdoctoral fellowship from the Swedish Society of Medical Research to H.B., a postdoctoral fellowship from Olle Engqvist Byggmästare to M.H., a PhD fellowship from Fundação para a Ciência e a Tecnologia to M.M.S.O., the Swedish Medical Society to H.B. and L.S.W., Groschinsky Foundation and Åke Wiberg Foundation to H.B. and L.S.W., the Swedish Cancer Society to M.B. and L.S.W., as well as the Swedish Research Council, the Swedish Childhood Cancer Fund, Karolinska Institutet, the European Commission 7th framework program, Åke Olsson foundation, Jeansson foundation, and Bergvall Foundation to L.S.W. L.S.W. is a Ragnar Söderberg fellow in Medicine.

Authorship contributions

S.O.B., M.B., and L.S.W. conceptualized the study, J.R., A.S., J.S.K., N.V.K., H.B. M.H., F.W., S.O.B., M.B., and L.S.W. designed the research, J.R., A.S., J.S.K., N.K., H.B., M.H., N.N., M.M.S.O., E.G., C.B.H., S.B., F.W, J.A., and L.S.W. performed the experiments and analyzed the data, N.N., J.D., A.J.T., C.L., H-E.C., O.W., S.O.B., M.B., and L.S.W. performed and supervised the analysis of patient samples and EBV transformation, J.R., A.S., and L.S.W. wrote the manuscript, and all authors edited the manuscript.

Disclosure of conflicts of interests

The authors declare no conflict of interests.

References

1. Borchmann S, Engert A. The genetics of Hodgkin lymphoma: an overview and clinical implications. Curr Opin Oncol. 2017;29(5):307-314.
2. Goldin LR, Bjorkholm M, Kristinsson SY, et al. Highly increased familial risks for specific lymphoma subtypes. Br J Haematol. 2009;146(1):91-94.
3. Kanzler H, Kuppers R, Hansmann ML, et al. Hodgkin and Reed-Sternberg cells in Hodgkin's disease represent the outgrowth of a dominant tumor clone derived from (crippled) germinal center B cells. J Exp Med. 1996;184(4):1495-1505.
4. Martin-Subero JI, Klapper W, Sotnikova A, et al. Chromosomal breakpoints affecting immunoglobulin loci are recurrent in Hodgkin and Reed-Sternberg cells of classical Hodgkin lymphoma. Cancer Res. 2006;66(21):10332-10338.
5. Bechtel D, Kurth J, Unkel C, et al. Transformation of BCR-deficient germinal-center B cells by EBV supports a major role of the virus in the pathogenesis of Hodgkin and posttransplantation lymphomas. Blood. 2005;106(13):4345-4350.
6. Mancao C, Altmann M, Jungnickel B, et al. Rescue of "crippled" germinal center B cells from apoptosis by Epstein-Barr virus. Blood. 2005;106(13):4339-4344.
7. Wang DZ, Li S, Hockemeyer D, et al. Potentiation of serum response factor activity by a family of myocardin-related transcription factors. Proc Natl Acad Sci U S A. 2002;99(23):14855-14860.
8. Miralles F, Posern G, Zaromytidou AI, et al. Actin dynamics control SRF activity by regulation of its coactivator MAL. Cell. 2003;113(3):329-342.
9. Cen B, Selvaraj A, Burgess RC, et al. Megakaryoblastic leukemia 1, a potent transcriptional coactivator for serum response factor (SRF), is required for serum induction of SRF target genes. Mol Cell Biol. 2003;23(18):6597-6608.
10. Selvaraj A, Prywes R. Expression profiling of serum inducible genes identifies a subset of SRF target genes that are MKL dependent. BMC Mol Biol. 2004;5:13.
11. Spencer JA, Misra RP. Expression of the serum response factor gene is regulated by serum response factor binding sites. J Biol Chem. 1996;271(28):16535-16543.
12. Hermann MR, Jakobson M, Colo GP, et al. Integrins synergise to induce expression of the MRTF-A-SRF target gene ISG15 for promoting cancer cell invasion. J Cell Sci. 2016;129(7):1391-1403.
13. Ma Z, Morris SW, Valentine V, et al. Fusion of two novel genes, RBM15 and MKL1, in the t(1;22)(p13;q13) of acute megakaryoblastic leukemia. Nat Genet. 2001;28(3):220-221.

14. Mercher T, Coniat MB, Monni R, et al. Involvement of a human gene related to the Drosophila spen gene in the recurrent t(1;22) translocation of acute megakaryocytic leukemia. Proc Natl Acad Sci U S A. 2001;98(10):5776-5779.

15. Medjkane S, Perez-Sanchez C, Gaggioli C, et al. Myocardin-related transcription factors and SRF are required for cytoskeletal dynamics and experimental metastasis. Nat Cell Biol. 2009;11(3):257-268.

16. Muehlich S, Hampl V, Khalid S, et al. The transcriptional coactivators megakaryoblastic leukemia 1/2 mediate the effects of loss of the tumor suppressor deleted in liver cancer 1. Oncogene. 2012;31(35):3913-3923.

17. Evelyn CR, Wade SM, Wang Q, et al. CCG-1423: a small-molecule inhibitor of RhoA transcriptional signaling. Mol Cancer Ther. 2007;6(8):2249-2260.

18. Hayashi K, Watanabe B, Nakagawa Y, et al. RPEL proteins are the molecular targets for CCG-1423, an inhibitor of Rho signaling. PLoS One. 2014;9(2):e89016.

19. Record J, Malinova D, Zenner HL, et al. Immunodeficiency and severe susceptibility to bacterial infection associated with a loss-of-function homozygous mutation of MKL1. Blood. 2015;126(13):1527-1535.

20. Bjorkholm M, Sjoberg J, Nygell UA, et al. Development of Hodgkin lymphoma in homozygotic triplets with constitutional deletion in MKL1. Blood. 2013;121(23):4807.

21. Nagy N, Adori M, Rasul A, et al. Soluble factors produced by activated CD4+ T cells modulate EBV latency. Proc Natl Acad Sci U S A. 2012;109(5):1512-1517.

22. Patarroyo M, Beatty PG, Nilsson K, Gahmberg CG. Identification of a cell-surface glycoprotein mediating cell adhesion in EBV-immortalized normal B cells. Int J Cancer. 1986;38(4):539-547.

23. Gronberg A, Halapi E, Ferm M, Petersson M, Patarroyo M. Regulation of lymphocyte aggregation and proliferation through adhesion molecule CD54 (ICAM-1). Cell Immunol. 1993;147(1):12-24.

24. Rothlein R, Springer TA. The requirement for lymphocyte function-associated antigen 1 in homotypic leukocyte adhesion stimulated by phorbol ester. J Exp Med. 1986;163(5):1132-1149.

25. Merk K, Bjorkholm M, Tullgren O, Mellstedt H, Holm G. Immune deficiency in family members of patients with Hodgkin's disease. Cancer. 1990;66(9):1938-1943.

26. Bjorkholm M, Holm G, Mellstedt H. Persisting lymphocyte deficiences during remission in Hodgkin's disease. Clin Exp Immunol. 1977;28(3):389-393.

27. Marits P, Wikstrom AC, Popadic D, Winqvist O, Thunberg S. Evaluation of T and B lymphocyte function in clinical practice using a flow cytometry based proliferation assay. Clin Immunol. 2014;153(2):332-342.

28. Shumilov A, Tsai MH, Schlosser YT, et al. Epstein-Barr virus particles induce centrosome amplification and chromosomal instability. Nat Commun. 2017;8:14257.

29. Wolf J, Kapp U, Bohlen H, et al. Peripheral blood mononuclear cells of a patient with advanced Hodgkin's lymphoma give rise to permanently growing Hodgkin-Reed Sternberg cells. Blood. 1996;87(8):3418-3428.

30. Verrills NM, Liem NL, Liaw TY, Hood BD, Lock RB, Kavallaris M. Proteomic analysis reveals a novel role for the actin cytoskeleton in vincristine resistant childhood leukemia--an in vivo study. Proteomics. 2006;6(5):1681-1694.

31. Rath N, Olson MF. Rho-associated kinases in tumorigenesis: re-considering ROCK inhibition for cancer therapy. EMBO Rep. 2012;13(10):900-908.

32. Gilles L, Bluteau D, Boukour S, et al. MAL/SRF complex is involved in platelet formation and megakaryocyte migration by regulating MYL9 (MLC2) and MMP9. Blood. 2009;114(19):4221-4232.

33. Smith EC, Thon JN, Devine MT, et al. MKL1 and MKL2 play redundant and crucial roles in megakaryocyte maturation and platelet formation. Blood. 2012;120(11):2317-2329.

34. Hanahan D, Weinberg RA. Hallmarks of cancer: the next generation. Cell. 2011;144(5):646-674.

35. Dorner M, Zucol F, Berger C, et al. Distinct ex vivo susceptibility of B-cell subsets to epstein-barr virus infection according to differentiation status and tissue origin. J Virol. 2008;82(9):4400-4412.

36. Heath E, Begue-Pastor N, Chaganti S, et al. Epstein-Barr virus infection of naive B cells in vitro frequently selects clones with mutated immunoglobulin genotypes: implications for virus biology. PLoS Pathog. 2012;8(5):e1002697.

37. Huang GL, Li BK, Zhang MY, et al. Allele loss and down-regulation of heparanase gene are associated with the progression and poor prognosis of hepatocellular carcinoma. PLoS One. 2012;7(8):e44061.

38. Shaul O. How introns enhance gene expression. Int J Biochem Cell Biol. 2017;91(Pt B):145-155.

39. Baarlink C, Wang H, Grosse R. Nuclear actin network assembly by formins regulates the SRF coactivator MAL. Science. 2013;340(6134):864-867.

40. Cheng X, Yang Y, Fan Z, et al. MKL1 potentiates lung cancer cell migration and invasion by epigenetically activating MMP9 transcription. Oncogene. 2015;34(44):5570-5581.

41. Hu Q, Guo C, Li Y, Aronow BJ, Zhang J. LMO7 mediates cell-specific activation of the Rho-myocardin-related transcription factor-serum response factor pathway and plays an important role in breast cancer cell migration. Mol Cell Biol. 2011;31(16):3223-3240.

42. Yamaguchi H, Condeelis J. Regulation of the actin cytoskeleton in cancer cell migration and invasion. Biochim Biophys Acta. 2007;1773(5):642-652.

43. Hamidi H, Pietila M, Ivaska J. The complexity of integrins in cancer and new scopes for therapeutic targeting. Br J Cancer. 2016;115(9):1017-1023.

44. Nguyen HG, Ravid K. Polyploidy: mechanisms and cancer promotion in hematopoietic and other cells. Adv Exp Med Biol. 2010;676:105-122.

45. Moulding DA, Moeendarbary E, Valon L, Record J, Charras GT, Thrasher AJ. Excess F-actin mechanically impedes mitosis leading to cytokinesis failure in X-linked neutropenia by exceeding Aurora B kinase error correction capacity. Blood. 2012;120(18):3803-3811.

46. Westerberg LS, Meelu P, Baptista M, et al. Activating WASP mutations associated with X-linked neutropenia result in enhanced actin polymerization, altered cytoskeletal responses, and genomic instability in lymphocytes. J Exp Med. 2010;207(6):1145-1152.

47. Rengstl B, Newrzela S, Heinrich T, et al. Incomplete cytokinesis and re-fusion of small mononucleated Hodgkin cells lead to giant multinucleated Reed-Sternberg cells. Proc Natl Acad Sci U S A. 2013;110(51):20729-20734.

48. Cuceu C, Hempel WM, Sabatier L, Bosq J, Carde P, M'Kacher R. Chromosomal Instability in Hodgkin Lymphoma: An In-Depth Review and Perspectives. Cancers. 2018;10(4).

49. Schwering I, Brauninger A, Klein U, et al. Loss of the B-lineage-specific gene expression program in Hodgkin and Reed-Sternberg cells of Hodgkin lymphoma. Blood. 2003;101(4):1505-1512.

50. Tiacci E, Doring C, Brune V, et al. Analyzing primary Hodgkin and Reed-Sternberg cells to capture the molecular and cellular pathogenesis of classical Hodgkin lymphoma. Blood. 2012;120(23):4609-4620.

Figure legends

Figure 1. The *MKL1* intronic deletion is associated with increased expression of *MKL1* and MKL1-induced genes. (A) Pedigree of genetically identical triplets whereof two have been diagnosed with HL. The *MKL1* intronic deletion is indicated by black color, HL with grey color, and undiagnosed with white color. Numbers indicate year of treatment. (B) Overview of *MKL1* indicating the deletion in intron 1. (C) MKL1 protein expression in primary lymphocytes by flow cytometry from two separate experiments. Experiment 1: Ctrl, HL0, and HL1. Experiment 2: C1 and HL2. Numbers indicate expression fold change normalized to ctrl and C1, respectively. (D) *MKL1* mRNA expression. (E) Representative image of MKL1 protein expression; in (F) normalized to GAPDH expression. (G) Expression of MKL1-induced genes by RT-qPCR. (D, F, G) show combined data from three experiments; experiments with primary lymphocytes (C) were performed once. For bar graphs, the dotted line indicates normalization to mean of C1 and C2. All panels display data from LCLs except (C), which displays primary lymphocyte data. Error bars represent the standard deviation of the measurements. Symbols represent technical replicates from three independent experiments in D and G, and single values from independent experiments in F. All data were analyzed using ANOVA with post-hoc Tukey test. *** $p<0.001$, **** $p<0.0001$

Figure 2. Increased actin content and actin-dependent spreading in HL0 and HL1 cells. (A) Phalloidin expression in primary lymphocytes by flow cytometry. Experiment 1: Ctrl, HL0, and HL1. Experiment 2: C1 and HL2. Numbers indicate expression fold change normalized to ctrl and C1, respectively. (B) Representative flow cytometry plot of G-actin and F-actin content in C2 and HL0 and (C-D) quantification of G- and F-actin content in control and triplets LCLs. (E) Immunocytochemistry of LCLs adhering to glass slides coated with fibronectin and anti-CD19 antibody. Spread cells defined as having lamellipodia-like structures and/or long protrusions. White arrowheads indicate examples of spread cells; black arrowheads indicate non-spread. Cells stained with phalloidin-Alexa488 (green color) and mounted in Vectashield Antifade Mounting Medium

with DAPI (blue color). Original magnification x400. (F) Proportion of spread LCLs. The experiment was repeated three times and cell spreading was determined each time in three separate fields of view. Total cells counted: C1: 800; C2: 1356; HL0: 1081; HL1: 1062; HL2: 983; and 200 cells or more were counted per sample per experiment. (G) Interference reflection microscopy of LCLs adhering to cover slips coated with fibronectin and anti-CD19 antibody. Original magnification x630. (H) Area of LCLs spread on coverslips. Total cells counted: C1: 119; C2: 109; HL0: 109; HL1: 131; HL2: 123. (C, D, F) show combined data from three experiments and (H) from two experiments. Experiments with primary lymphocytes (A) were performed once. (B) shows representative histograms and (E, G) show representative images. For bar graphs, the dotted line indicates normalization to mean of C1 and C2. All panels display data from LCLs except (A), which displays primary lymphocyte data. Error bars represent the standard deviation of the measurements. Symbols represent technical replicates from three independent experiments in F, and pooled single values from three independent experiments in H. All data were analyzed using ANOVA with post-hoc Tukey test. * $p<0.05$, ** $p<0.01$, *** $p<0.001$, **** $p<0.0001$

Figure 3. HL0 cells display decreased aggregation and reduced CD11a integrin expression. (A) Aggregation of LCLs, representative images. (B) Average area of aggregates observed in (A). (C) Representative flow cytometry plots of total CD11a surface expression in LCLs. (D) Quantification of CD11a surface expression as seen in (C). (E-F) Quantification of inactive CD11a and CD54 surface expression as seen in Figure S3. (G) Expression of *ITGAL* (CD11a) by RT-qPCR. (H) Quantification of total CD11a protein expression. (B, D-F) show combined data from three experiments. (G-H) show combined data from two experiments. For bar graphs, the dotted line indicates normalization to the mean of C1 and C2. All panels display data from LCLs. Error bars represent the standard deviation of the measurements. Symbols represent technical replicates from three independent experiments in G, and single values from three independent experiments in

F. All data were analyzed using ANOVA with post-hoc Tukey test. * $p<0.05$, ** $p<0.01$, *** $p<0.001$

Figure 4. HL0 cells display increased proliferation and genomic instability. (A) Expression of proliferation marker Ki-67 by flow cytometry on primary B cells cultured 48 hours with IL-4 and anti-CD40 antibodies. Numbers indicate expression fold change normalized to the mean of C1 and C2. (B) DNA synthesis rate as measured by radiation from incorporated ^{3}H-thymidine after 48 hours. (C) Cell cycle phase proportions (G0/G1, S and G2/M) determined by Hoechst 33342 staining, measured by flow cytometry (representative histograms). Left graph shows how Y-axis was cut to allow for emphasized visualization of hyperploid cells with >4n of DNA content, quantified in (D). (E) Comparison of mononuclear (indicated by white arrowhead) and multinuclear (black arrowhead) LCLs. White color: DAPI; green color: phalloidin-Alexa488. (F) Proportion of multinucleated LCLs, as assessed by manual microscopical counting of nuclei stained with DAPI. Numbers indicate counted cells for each sample. (G) Telomere-FISH on chromosomes in metaphase. Representative images of a normal cell with 46 chromosomes and a hyperploid cell with 92 chromosomes; insets show magnified representative chromosomes. Original magnification x1000. Chromosomes hybridized with TelG-Cy3 PNA probe (red color) and mounted in Vectashield Antifade Mounting Medium with DAPI (blue color). (H) Proportion of metaphases with a hyperploid amount of chromosomes (>46). Numbers indicate counted metaphases for each sample. (I) Subcutaneous injection of C1 and HL0 LCLs in NSG mice and measurement of tumor mass at day 9. Each circle represents one mouse. Right subpanel: representative image of tumor mass assessed at endpoint. Black arrowhead indicates angiogenesis. (A) shows data from one experiment; (B, D, F, H) show combined data from three experiments; (I) shows combined data from two experiments. For bar graphs, the dotted line indicates normalization to the mean of C1 and C2. All panels display data from LCLs except (A), which displays primary B cell data. Error bars represent the standard deviation of the measurements. All data were analyzed using ANOVA with

post-hoc Tukey test, except (I) that was analyzed using t-test. * $p<0.05$, ** $p<0.01$, *** $p<0.001$, **** $p<0.0001$

Figure 5. HL1 display two distinct populations of cells of which one shows an HL0 phenotype. (A) *i)* Representative flow cytometry plots from eight experiments showing gating on LCLs using SSC vs FSC. *ii)* CD11a expression in HL1 cells. HL1 cells were sorted using according to CD11a surface expression resulting in the two populations CD11a low and CD11a high cells shown in *iii)* and *iv)*, respectively. (B) MKL1 expression in CD11a low and CD11a high LCLs was evaluated by Western blot. Left subpanel: representative Western blot showing MKL1 expression in CD11a low on high cells. Right subpanel: quantification by densitometry of MKL1 relative expression over GAPDH in four independent experiments. (C) Proportion of spread LCLs. CD11a low and high cells were let to spread on glass slides coated with fibronectin and anti-CD19 antibody. The experiment was repeated two times and cell spreading was determined each time in three separate fields of view. Total cells counted: CD11a low: 689; CD11a high: 579; and 200 cells or more were counted per sample per experiment. (D) Aggregation of CD11a low and high LCLs, representative images. (E) Average area of aggregates. Results from three independent experiments. (F) Cell concentration of CD11a low and CD11a high LCLs over 8 days. Results from five independent experiments. (G) Left subpanel: CD11a low or CD11a high LCLs were injected subcutaneous in NSG mice and the tumor size was measured 15 days later. Right subpanel: quantification of the tumor size in NSG mice injected with either CD11a low or high LCLs. Results from three independent experiments. (H) Microscopy for the L1236 HL cell line. Green: F-actin; blue: nuclear stain. CD11a expression by flow cytometry. Symbols represent single values from four independent experiments in B and F, and technical replicates from two and three independent experiments in C and G respectively. Error bars represent the standard deviation of the measurements. All data were analyzed using t-test. * $p<0.05$, *** $p<0.001$

Figure 6. Inhibition of MKL1 activity in HL0 cells induces a phenotype similar to control cells. (A) Left and middle subpanels: Representative flow cytometry plots showing gating for size, granularity, and DAPI fluorescence intensity as a measure of the proportion of dead cells of HL0 LCLs treated with 10μM of CCG-1423 for 24 hours. Right subpanel: quantification of cell death of HL0 cells treated with DMSO or CCG-1423 for 24 hours. Representative graph of three independent experiments. (B) Representative image of MKL1 protein expression in HL0 LCLs treated with DMSO or CCG-1423 for 24 hours. (C) Quantification of MKL1 expression levels normalized to GAPDH in HL0 LCLs treated with DMSO or CCG-1423 for 24 hours. Results from three independent experiments. (D) Expression of *SRF* mRNA by RT-qPCR in HL0 LCLs treated with DMSO or CCG-1423 for 24 hours. Results from three independent experiments. (E) Proportion of spread HL0 LCLs after treatment with DMSO or CCG-1423 for 48 hours. Experiment was repeated two times and cell spreading was determined each time in three separate fields of view. Total cells counted: DMSO: 541; 2 μM: 517; 5 μM: 454; 10 μM: 271; and 100 cells or more were counted per sample per experiment. (F) Aggregation in culture of HL0 LCLs treated with DMSO or CCG-1423 for 24 hours. More than 15 fields were randomly chosen for quantification. Original magnification x40. (G) Quantification of aggregation observed in (F) using ImageJ. Data representative of two independent experiments. Numbers indicate counted aggregates for each sample. (H) DNA synthesis rate in HL0 LCLs as measured by radiation from incorporated ^{3}H-thymidine after 48 hours of treatment with DMSO or CCG-1423. (I) HL0 LCLs were injected in NSG mice. From day 6, 50μL of DMSO or 10μM of CCG-1423 was injected intratumorally daily for 6 days. Tumor size was measured on day 12. Error bars represent the standard deviation of the measurements. Symbols represent single values from three independent experiments in C, mean values in D, and technical replicates from two independent experiments in C and G. All data were analyzed using ANOVA with post-hoc Tukey test. * $p<0.05$, ** $p<0.01$, *** $p<0.001$, **** $p<0.0001$

Figure 1

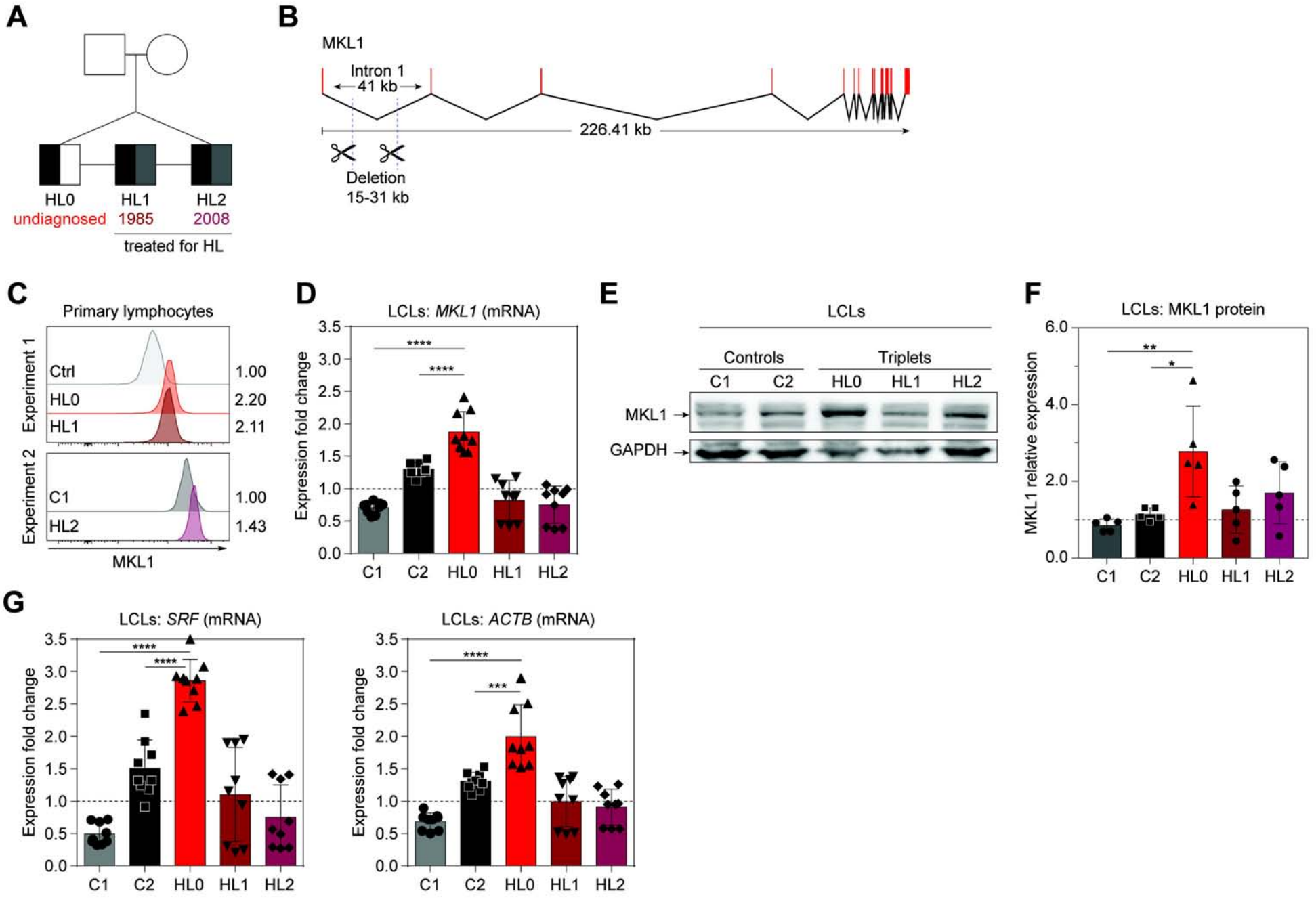
A
HL0
undiagnosed
HL1
1985
HL2
2008
treated for HL
B
MKL1
Intron 1
41 kb
226.41 kb
Deletion
15-31 kb
C
Primary lymphocytes
Experiment 1
Ctrl
HL0
HL1
1.00
2.20
2.11
Experiment 2
C1
HL2
1.00
1.43
MKL1
D
LCLs: MKL1 (mRNA)
Expression fold change
C1
C2
HL0
HL1
HL2
E
LCLs
Controls
Triplets
C1
C2
HL0
HL1
HL2
MKL1
GAPDH
F
LCLs: MKL1 protein
MKL1 relative expression
G
LCLs: SRF (mRNA)
LCLs: ACTB (mRNA)

Figure 2

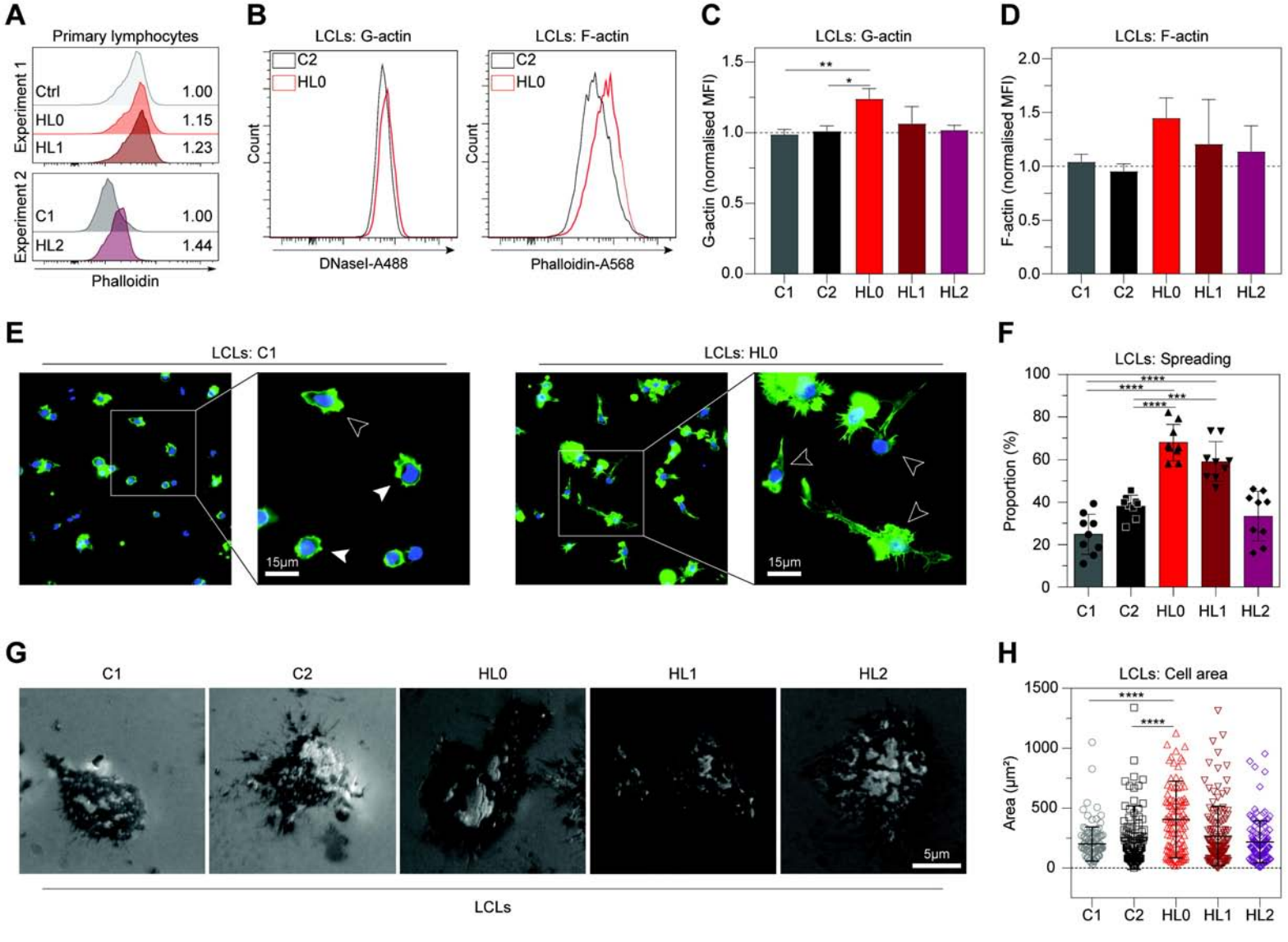
A
Primary lymphocytes
Experiment 1
Ctrl
1.00
HL0
1.15
HL1
1.23
Experiment 2
C1
1.00
HL2
1.44
Phalloidin
B
LCLs: G-actin
C2
HL0
Count
DNaseI-A488
LCLs: F-actin
C2
HL0
Count
Phalloidin-A568
C
LCLs: G-actin
G-actin (normalised MFI)
1.5
1.0
0.5
0.0
**
*
C1
C2
HL0
HL1
HL2
D
LCLs: F-actin
F-actin (normalised MFI)
2.0
1.5
1.0
0.5
0.0
C1
C2
HL0
HL1
HL2
E
LCLs: C1
15µm
LCLs: HL0
15µm
F
LCLs: Spreading
Proportion (%)
100
80
60
40
20
0
****
****
****
***
C1
C2
HL0
HL1
HL2
G
C1
C2
HL0
HL1
HL2
5µm
LCLs
H
LCLs: Cell area
Area (µm²)
1500
1000
500
0
****
****
C1
C2
HL0
HL1
HL2

Figure 3

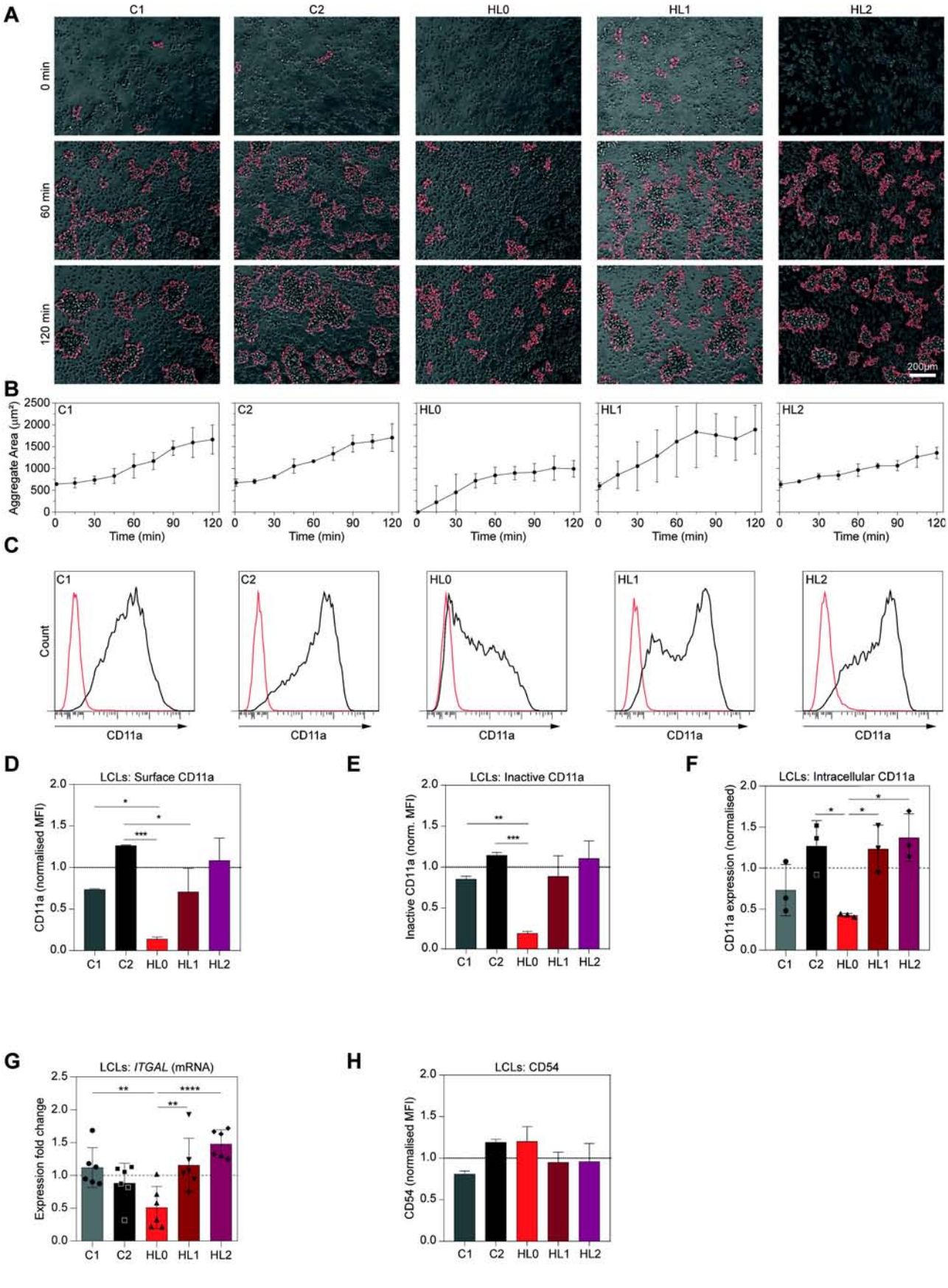
A
C1
C2
HL0
HL1
HL2
0 min
60 min
120 min
200µm
B
Aggregate Area (µm²)
Time (min)
C
Count
CD11a
D
LCLs: Surface CD11a
CD11a (normalised MFI)
E
LCLs: Inactive CD11a
Inactive CD11a (norm. MFI)
F
LCLs: Intracellular CD11a
CD11a expression (normalised)
G
LCLs: ITGAL (mRNA)
Expression fold change
H
LCLs: CD54
CD54 (normalised MFI)

Figure 4

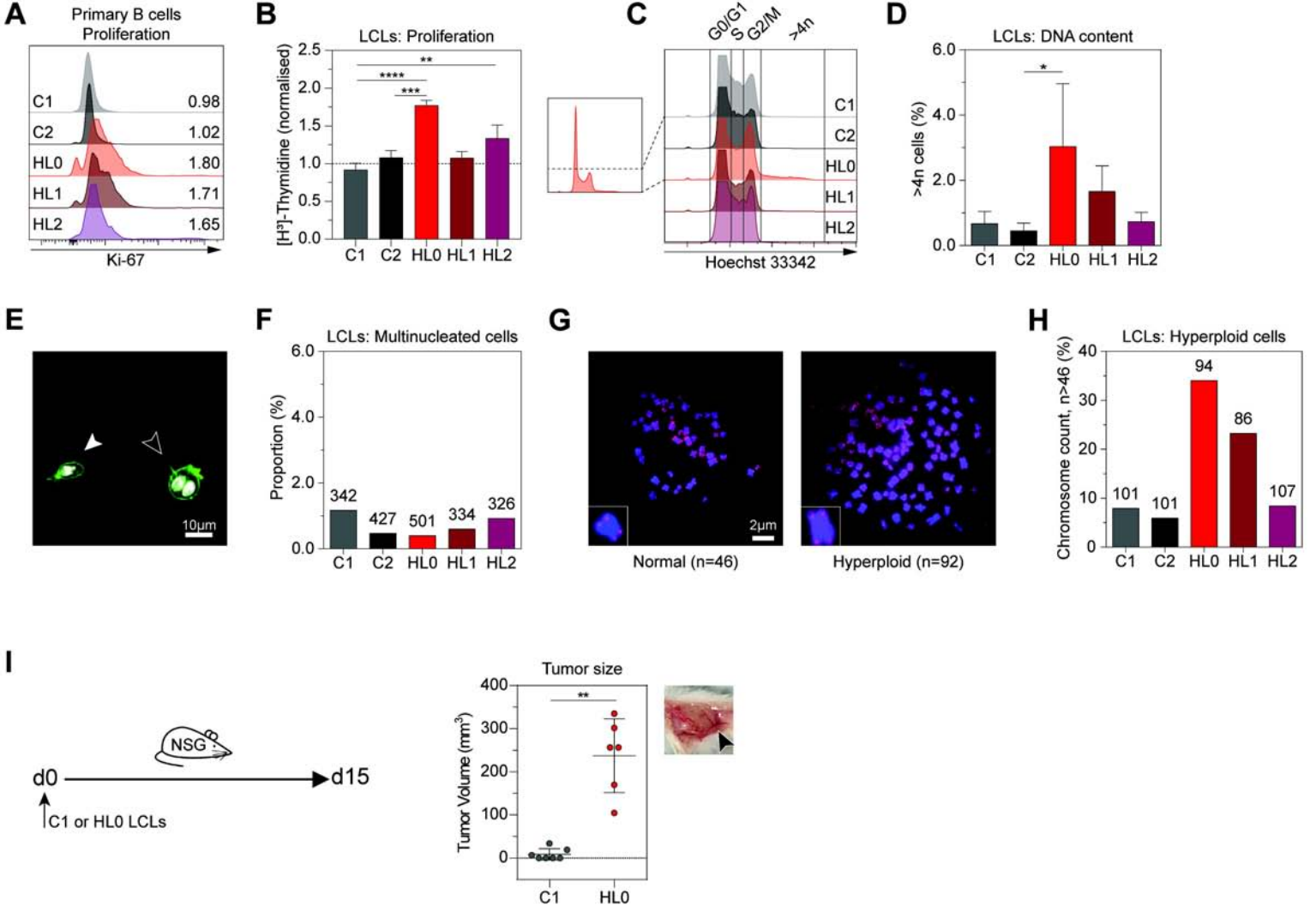
A
Primary B cells Proliferation
C1 0.98
C2 1.02
HL0 1.80
HL1 1.71
HL2 1.65
Ki-67
B
LCLs: Proliferation
[H³]-Thymidine (normalised)
C1 C2 HL0 HL1 HL2
C
G0/G1 S G2/M >4n
C1 C2 HL0 HL1 HL2
Hoechst 33342
D
LCLs: DNA content
>4n cells (%)
C1 C2 HL0 HL1 HL2
E
10µm
F
LCLs: Multinucleated cells
Proportion (%)
342 427 501 334 326
C1 C2 HL0 HL1 HL2
G
2µm
Normal (n=46)
Hyperploid (n=92)
H
LCLs: Hyperploid cells
Chromosome count, n>46 (%)
101 101 94 86 107
C1 C2 HL0 HL1 HL2
I
NSG
d0
d15
C1 or HL0 LCLs
Tumor size
Tumor Volume (mm³)
C1 HL0

Figure 5

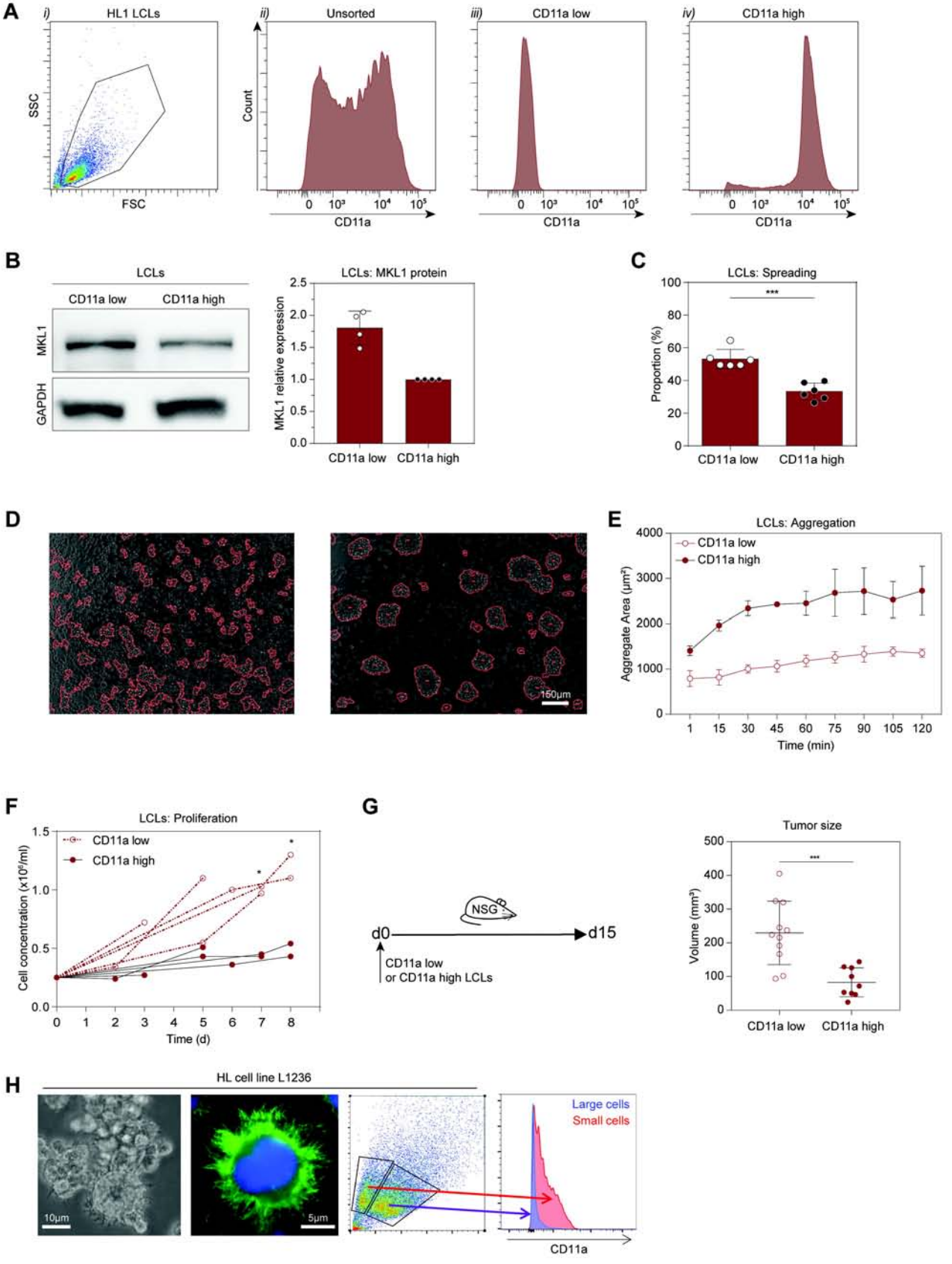
A
i)
HL1 LCLs
SSC
FSC
ii)
Unsorted
Count
CD11a
iii)
CD11a low
iv)
CD11a high
B
LCLs
CD11a low
CD11a high
MKL1
GAPDH
LCLs: MKL1 protein
MKL1 relative expression
C
LCLs: Spreading
Proportion (%)
***
D
150µm
E
LCLs: Aggregation
CD11a low
CD11a high
Aggregate Area (µm²)
Time (min)
F
LCLs: Proliferation
Cell concentration (x10⁶/ml)
Time (d)
G
NSG
d0
d15
CD11a low
or CD11a high LCLs
Tumor size
Volume (mm³)
H
HL cell line L1236
10µm
5µm
Large cells
Small cells
CD11a

Figure 6

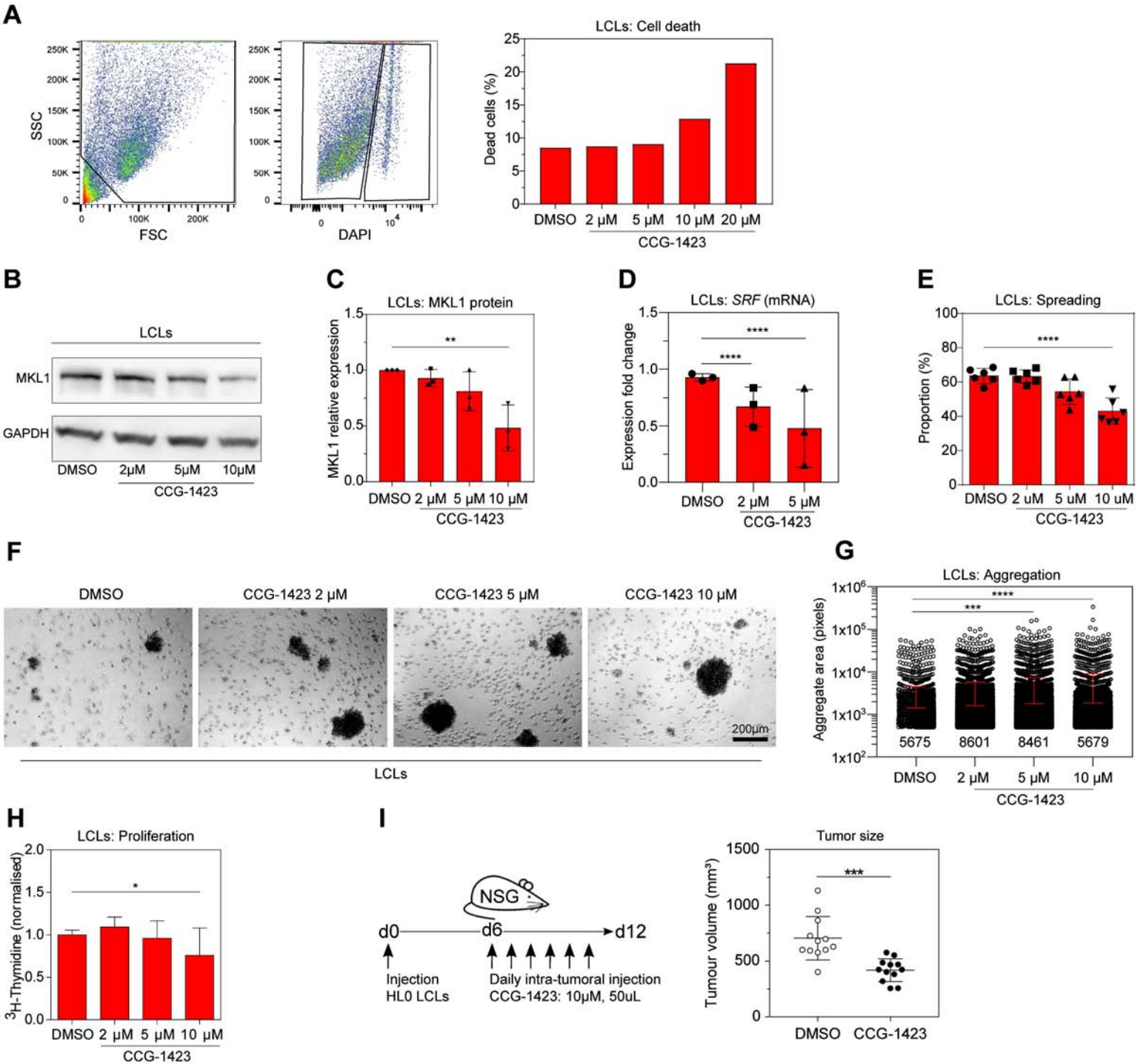
A
SSC
FSC
DAPI
LCLs: Cell death
Dead cells (%)
DMSO 2 µM 5 µM 10 µM 20 µM
CCG-1423
B
LCLs
MKL1
GAPDH
DMSO 2µM 5µM 10µM
CCG-1423
C
LCLs: MKL1 protein
MKL1 relative expression
DMSO 2 µM 5 µM 10 µM
CCG-1423
D
LCLs: SRF (mRNA)
Expression fold change
DMSO 2 µM 5 µM
CCG-1423
E
LCLs: Spreading
Proportion (%)
DMSO 2 uM 5 uM 10 uM
CCG-1423
F
DMSO
CCG-1423 2 µM
CCG-1423 5 µM
CCG-1423 10 µM
200µm
LCLs
G
LCLs: Aggregation
Aggregate area (pixels)
5675 8601 8461 5679
DMSO 2 µM 5 µM 10 µM
CCG-1423
H
LCLs: Proliferation
3H-Thymidine (normalised)
DMSO 2 µM 5 µM 10 µM
CCG-1423
I
NSG
d0 d6 d12
Injection
HL0 LCLs
Daily intra-tumoral injection
CCG-1423: 10µM, 50uL
Tumor size
Tumour volume (mm3)
DMSO CCG-1423

Extended Methods

Human blood samples

Whole blood samples were obtained from the triplets and age-matched controls after informed consent was given. This study was performed according to the principles expressed in the Helsinki Declaration and with approval from the local ethics committee (Dnr 2015/416-31). For analysis of primary cells, the first experiment included samples from HL0, HL1, and ctrl (not used for EBV-transformation) collected in February 2015 and the second experiment HL2 and C1, collected in May 2015. To establish EBV-transformed LCLs, PBMCs from HL0, HL1, and HL2, and two age- and sex-matched controls (C1 and C2), all collected in November 2015, were cultured with supernatant of the virus-producing B95-8 line (1).

Clinical status of patients

HL0 has remained free from HL including the time of blood sampling. He suffered one stroke in 2009 and another in 2010. However, he still (2019) remains free from HL. The triplet HL1 was diagnosed in 1985 at age 40 with stage IIIA HL of Epstein-Barr virus (EBV)–positive mixed cellularity subtype. He has been treated with mustargen, oncovin, procarbazine, prednisone/adriamycin, bleomycin, vinblastine, and dacarbazine chemotherapy. The triplet HL1 had enjoyed a 31-year continuous first complete remission at the time of blood sampling. To date he remains free from HL but underwent surgery for a prostate cancer in 2011. He suffers from cardiovascular disease. The triplet HL2 developed stage IIIB HL in 2008. His tumor was EBV-positive and of nodular sclerosis (NS) subtype. A complete and lasting remission was achieved following adriamycin, bleomycin, vinblastine and dacarbazine chemotherapy. The triplet HL2 died from cardiac insufficiency in January 2017. There were no clinical or laboratory signs of HL at the time of blood sampling or death.

Mice

NOD/SCID-IL2rγ^{null} (NSG) mice (2) were bred and maintained at the animal facility of the Department of Microbiology, Tumor and Cell Biology at Karolinska Institutet under specific pathogen-free conditions. Female mice were used 6-12 weeks of age and all animal experiments were performed after approval from the local ethics committee (the Stockholm District Court, permit N77/13 and N272/14).

Flow-cytometric assay of specific cell-mediated immune response in activated whole blood (FASCIA)

Whole blood samples were subjected to Flow-cytometric Assay for Specific Cell-mediated Immune-response in Activated whole blood (FASCIA) (3) to examine the capacity to form blast cells upon stimulation with different antigens. Heparinized whole blood was diluted 1:10 in RPMI-1640 supplemented with 10-20 % fetal calf serum (FCS), L-glutamine, penicillin-streptomycin, and Na-pyruvate (complete RPMI). The blood-medium mixture was stimulated with medium alone or with medium containing Phytohemagglutinin, Pokeweed mitogen, Concanavalin A, Prevenar vaccine, Tetanus toxin, Influenza A vaccine, PPD, Candida, Staphylococcal enterotoxin A/B, or Varicella zoster virus and cultured for 7 days at 37 °C with 5 % CO_2. At day 7, cells were stained with CD3-FITC/CD4-PE Simultest mix (BD Biosciences, San Jose, CA, USA) and in samples with Pokeweed mitogen with CD19-PC7 (Beckman Coulter, Brea, CA, USA). Blast numbers were acquired during 80 seconds using a FC500 or Navios flow cytometer (Beckman Coulter). To obtain an absolute number of proliferating (blast) cells per µL whole blood, Trucount (BD Biosciences) tubes were used (3). Table 1 shows blast cell numbers at day 7.

Primary B cell isolation and culture

Ten mL of whole blood was diluted 1:4 with 0.9 % NaCl and underlaid with 10 mL of Ficoll-Paque PLUS (GE Healthcare Life Sciences, Marlborough, MA, USA); after centrifuging at 400 *g* for 40 minutes at room temperature (rt), the peripheral blood mononuclear cell (PBMC) layer was aspirated and washed twice with Ca^{2+} and Mg^{2+}-free Hank's balanced salt solution (ThermoFisher Scientific, Waltham, MA, USA). B cells were isolated using the CD19 MicroBeads kit (Miltenyi Biotec, Bergisch Gladbach, Germany), according to the company protocol. MACS buffer was prepared with phosphate-buffered saline (PBS), pH 7.2, 0.5 % bovine serum albumin (BSA), and 2 mM EDTA. Cells were suspended in 80 µL of buffer and 20 µL of CD19 MicroBeads per 10^7 cells, incubated for 15 minutes at 4 °C, and subsequently washed with buffer. Labeled cells were separated by passing cell suspension through MACS® MS columns (Miltenyi Biotec). For primary cell culture, B cells were suspended at $0.5x10^6$ cells/ml in complete RPMI with 30 ng/mL human IL-4, (Peprotech, London, UK), and 3 µg/mL anti-human CD40 (S2C6; MabTech, Cincinnati, OH, USA).

EBV transformation

For the establishment of EBV-transformed LCLs, PBMCs from HL0, HL1, and HL2, and two age- and sex-matched controls (C1 and C2) were isolated from blood by Ficoll-Paque gradient separation. B cells were infected with EBV by incubating the PBMCs with supernatant of the virus-producing B95-8 line for 90 minutes at 37 °C (1). Thereafter the cells were washed, re-suspended in complete RPMI-1640 medium and cultured until stable LCLs were obtained. Cyclosporin A was added to the medium (0.5 µg/mL) for the first 4 weeks in order to inhibit EBV-specific T cells. LCLs were cultured in complete RPMI at $0.3–1.5x10^6$ cells/mL.

Reverse transcriptase-quantitative real-time polymerase chain reaction (RT-qPCR)

Total RNA from LCLs was isolated with the RNeasy kit (QIAGEN GmbH, Hilden, Germany). Each sample was treated with RNAse-free DNAse (QIAGEN) and RNA concentration was measured with the NanoDrop 2000 (ThermoFisher Scientific). The visual quality control for RNA integrity and purity was performed by 1 % UltraPure Agarose (ThermoFisher Scientific), 1x TAE gel electrophoresis analysis. Gel images were created with the ImageQuant LAS4000 Image System using the ImageQuant LAS4000 Control Software (GE Healthcare). Two µg of total RNA per sample was used for each cDNA synthesis reaction together with SuperScript II Reverse Transcriptase (ThermoFisher Scientific). The following primer pairs was used; MKL1-forward 5'-ACTAGCCGATGACCTCAATGA-3' and MKL1-reverse 5'-TTCACCTGGCCCACAATGATG-3'; SRF-forward 5'-CGAGATGGAGATCGGTATGGT-3' and SRF-reverse 5'-GGGTCTTCTTACCCGGCTTG-3'; ACTB-forward 5'-CATGTACGTTGCTATCCAGGC-3' and ACTB-reverse 5'-CTCCTTAATGTCACGCACGAT-3'; ITGAL-forward 5'-TGCTTATCATCATCACGGATGG-3' and ITGAL-reverse 5'-CTCTCCTTGGTCTGAAAATGCT-3'. RT-qPCR reactions were performed using SsoAdvanced Universal SYBR Green Supermix kit (Bio-Rad, Hercules, CA USA) in the C1000/CFX96 RT-qPCR System (Bio-Rad). Gene expression data were analyzed using Excel (Microsoft, Redmond, WA, USA). The arithmetic mean Ct of the triplicate, ΔCt, and RQ values were calculated, and then RQ values were normalized by average RQ of healthy controls (C1 and C2). The normalized RQ mean of biological replicates was determined and shown as "Expression fold change" with error bars representing the average deviation.

Western blotting

Cell lysates from LCLs were obtained by incubating $2x10^6$ cells for 30 minutes at 4 °C in 100 µL of NP-40 based buffer (NaCl: 150 mM, NP40: 0.5 %, tris(hydroxymethyl)aminomethane

(Tris)-Cl, pH 8.0: 50 mM) or radioimmunoprecipitation assay buffer (G-Biosciences, St. Louis, MO, USA) containing a protease inhibitor cocktail (Sigma-Aldrich, St. Louis, MO, USA). During the lysis, the samples were vortexed every 10 minutes. The samples were then centrifuged at 13,000 rpm at 4 °C for 10 minutes before the supernatant was collected and mixed with Laemmli sample buffer in a 1:1 ratio and boiled at 95 °C for 10 minutes. Cell lysates (20 µL per well) were separated on Bolt 4–12 % Bis-Tris Plus polyacrylamide gels (ThermoFisher Scientific) in 1x MOPS (3-[N-morpholino]propanesulfonic acid) SDS Running Buffer (ThermoFisher Scientific). SeeBlue® Plus2 Pre-stained Protein Standard (ThermoFisher Scientific) was included as a size marker. The membrane was then blocked with 5 % BSA/PBS-Tween 0.1 % (PBST) solution before being incubated overnight at 4 °C in 5 % BSA/PBST with the anti-MKL1 antibodies sc-21558 (Santa Cruz Biotechnology, Dallas, TX, USA) or HPA030782 (Sigma-Aldrich) at 1:500 and 1:250, respectively. The membrane was then incubated for 1 hour at rt with HRP-conjugated secondary antibodies mouse anti-rabbit (sc-2357; Santa Cruz Biotechnology) or mouse anti-goat (sc-2354; Santa Cruz Biotechnology) in 5 % BSA/PBST at 1:5000 and 1:10,000 respectively. The blot membrane was then developed with PIERCE ECL Western Blotting substrate and blot images were acquired using the ImageQuant LAS4000 Image system and ImageQuant LAS4000 Control Software (GE Healthcare). An anti-GAPDH antibody (sc-25778; Santa Cruz Biotechnology) was used as loading control.

Flow cytometry

Flow cytometry was performed on PBMCs, LCLs, and cultured primary B cells using the LSRFortessa X-20 (BD Biosciences) and results were processed using FlowJo v10 software (TreeStar Inc., St. Ashland, Oregon, USA). Whole blood was diluted 1:20 in FACS Lysing solution (BD Biosciences) to lyse erythrocytes, washed twice with PBS after 5 minutes of

incubation. Cultured primary B cells and LCLs were washed with PBS and analyzed in single-cell suspensions.

Analysis of primary lymphocytes was performed by first incubating the cells for 10 minutes in PBS with FcBlock (1:200; BD Biosciences) for blocking together with the Aqua Dead Cell Stain (1:300; ThermoFisher Scientific) diluted at 1:300 to determine living cells. The cells were then fixed and permeabilized with the Foxp3/Transcription Factor Fixation/Permeabilization kit (ThermoFisher Scientific). Proliferation was assessed using an anti-human Ki-67-Alexa647 antibody (Biolegend) at 1:100 in 5 % BSA/PBS for 30 minutes at rt.

For MKL1 expression in primary B cells, cells were fixed with Fix/Perm solution (BD Bioscience) for 30 minutes before being stained with rabbit anti-human MKL1 at 1:50 (Sigma-Aldrich) for 30 minutes at rt. The cells were then incubated with a goat Alexa568-conjugated anti-rabbit antibody at 1:1000 (ThermoFisher Scientific) for 30 minutes. To determine the F-actin content, the cells were, after fixation and permeabilization, incubated with a solution of biotinylated phalloidin (ThermoFisher Scientific) at 1:1000 for 30 minutes at rt. The cells were then incubated with streptavidin-APC/Cy7 (BioLegend, San Diego, CA, USA) at 1:1000 for 30 minutes at rt. All steps above were followed by three washes with PBS.

Cell cycle analysis of LCLs was performed by collecting cells directly from culture and labelling them with 5 µg/mL Hoechst-33342 (ThermoFisher Scientific) in PBS for 30 minutes at 37 °C, and then washed twice in PBS before analysis.

To determine integrin expression at the cell surface, LCLs were collected and washed twice with ice-cold PBS before being resuspended in 100 µL of 2 % BSA/FcBlock (BD Bioscience)

in PBS and incubated for 20 minutes on ice. The cells were then stained for 30 minutes on ice with an anti-human CD11a antibody (TS2/4; Biolegend) for total CD11a expression, or an anti-human CD11a antibody (Hl111; Biolegend) for inactive/closed conformation-CD11a expression, or the anti-human CD54 antibody (Biolegend). The cells were incubated with an anti-mouse-Alexa647 antibody (ThermoFisher Scientific) for 30 minutes on ice before being analyzed. All staining steps were followed by two washes with ice-cold PBS and one wash with ice-cold 2 % BSA/PBS.

To determine F- and G-actin content in two LCL samples side by side, one sample was incubated with an anti-human CD54 antibody (Biolegend) for 30 minutes on ice. The cells were washed three times with ice-cold PBS before being incubated with an anti-mouse-Alexa647 antibody (ThermoFisher Scientific) for 30 minutes on ice. The labeled sample were mixed with an unlabeled sample in the same tube and then fixed using 4 % formaldehyde (FA) for 20 minutes and permeabilized using 0.1 % Triton X-100 (Sigma-Aldrich) for 10 minutes. PBS containing 2 % BSA was used as blocking agent for 30 minutes before the cells were stained for 30 minutes with a 2 % BSA/PBS solution with DNaseI-Alexa488 (ThermoFisher Scientific) and phalloidin-Alexa568 (ThermoFisher Scientific) at 1:1000 and 1:400, respectively. The cells were washed three times for 5 minutes with PBS before being analyzed.

Fluorescence-activated cell sorting

HL1 cells were sorted according to their CD11a expression. $10x10^6$ cells or more were collected and washed twice with ice-cold PBS before being resuspended in 2 % BSA/FcBlock (1:50, BD Bioscience) in PBS and incubated for 20 minutes on ice. Then, cells were stained for CD11a for 30 minutes on ice with an anti-human CD11a antibody (TS2/4; Biolegend). Subsequently, cells were incubated with Alexa647-conjugated anti-mouse antibody

(ThermoFisher Scientific) for 30 minutes on ice before being resuspended in 1 % FBS/Gey's balanced salt solution (GBSS). The cells were sorted using a FACSAria (BD Biosciences) and collected in 50 % FBS/GBSS.

Immunocytochemistry

Glass slides were coated with a fibronectin solution (50 µg/mL in PBS; Invitrogen) for 1 hour at 37 °C (ThermoFisher Scientific) and then with anti-CD19 antibody (BD Biosciences) (20 µg/mL in PBS) for 1 hour at 37 °C before being washed twice with PBS. Cells in complete RPMI were seeded at 10^6 cells/mL and were let to adhere for 1 hour and 40 minutes at 37 °C. Cells were then fixed with 3.7 % FA for 15 minutes and permeabilized with 0.1 % Triton X-100 (Sigma-Aldrich) for 15 minutes. 10 % FCS/PBS was used for blocking for 1 hour before F-actin was stained with phalloidin-Alexa488 (ThermoFisher Scientific) at 1:500 in 10 % FCS/PBS. Each step listed above was followed by three 5-minute PBS washes. Slides were mounted with Vectashield Antifade Mounting Medium with DAPI (Vector Laboratories, Burlingame, CA, USA). The cells were imaged using a Leica DMRE epi-fluorescence microscope equipped with 25x/0.75 PL-FL and 40x/1.00-0.50 PL-FL objectives. Images were acquired at rt using the Hamamatsu C4880 camera and the HiPic 32 software (Hamamatsu, Shizuoka, Japan). Original magnification x400. Brightness and contrast were adjusted using ImageJ/FIJI(4). Spread cells were defined as having lamellipodia-like structures and/or long protrusions and manually counted. For nuclei counting, cell borders were determined by phalloidin staining and nuclei identified by DAPI (4',6-diamidino-2-phenylindole) staining.

Interference reflection microscopy

To determine cell adhesion area, $0.25x10^6$ LCLs were transferred to glass cover slips coated with 50 µg/mL fibronectin (Invitrogen) and 5 µg/mL purified anti-CD19 antibody (BD

Biosciences) and thereafter incubated for 1 hour and 40 minutes at 37 °C. Afterwards, cells were fixed with 1.3 % FA and mounted with Aqua Poly/Mount (Polysciences Inc., Taipei, Taiwan). Cells were assessed with interference reflection microscopy using a Zeiss Axio Observer Z1 microscope equipped with a Zeiss analyzer slider D/A, 360° rotatable position, polarizer and a Hg/Mercury-lamp. Pictures were acquired using a 63x oil-immersion lens and the ZEN software (Zeiss, Oberkochen, Germany). ImageJ was used for data analysis of adhesion area, following normalization of brightness and contrast by setting the range equal to all pictures within the experiment, subtraction of the background using a 50 pixel rolling ball radius and normalization of threshold.

Time-lapse imaging of cell aggregation

LCLs were washed twice with PBS and resuspended at $1.6x10^6$ cells/mL in RPMI-1640 containing 0.5 % BSA and 20 mM HEPES (N-2-hydroxyethylpiperazine-N'-2-ethanesulfonic acid). 100 µL of cell suspension per sample was seeded in a flat bottom 96-well plate. The plate was placed in the microscope environmental chamber at 37 °C, incubated for 10 minutes, whereby 100 µL of warm medium was added to the wells and incubated for 10 minutes. Aggregation was imaged every 2 minutes at 37 °C with 5 % CO_2 using a Zeiss CellObserver Z1 equipped with a EC Plan-Neofluar 10x/0.30 Ph1 objective and a Zeiss Axiocan MR R3 camera. Images were processed using ImageJ/FIJI. To detect aggregates, the “Find edges” function and a Gaussian filter (Sigma: 4) were applied resulting in the aggregates displayed as bright objects over a dark background. A signal threshold was then applied to generate a binary image and to locate aggregates. To discriminate aggregates from single cells that were not filtered out by the threshold, aggregates of 5 cells or more were detected with the “Analyze particles” function (size filter: 500 μm^2–∞). Results were analyzed in Microsoft Excel (Microsoft, Redmond, Washington, USA).

DNA synthesis assessment

LCLs were seeded at $3x10^5$ cells/mL and cultured for 48 hours with a 2.5 μCi/mL ^{3}H-thymidine (1 Ci = 37 GBq) pulse the last 20 hours. Cells were harvested onto a membrane, scintillation liquid was added, and incorporated radioactivity was measured using a Wallac microplate scintillation counter (Wallac Oy, Turku, Finland).

Metaphase preparation and telomere-FISH

Telomere-fluorescent in situ hybridization was performed as previously described (5). LCLs in culture were seeded at 10^6 cells/mL and arrested in metaphase with the addition of 0.1 μg/mL colcemide (ThermoFisher Scientific) for 5 hours at 37 °C. After PBS washing, 10 mL of 0.075 M KCl was added slowly to the cells to allow them to swell, while vortexing them gently to avoid aggregation. Cells were incubated at 37 °C for 15 minutes whereafter two drops of fixative consisting of 3:1 of methanol and glacial acetic acid (Sigma-Aldrich) were added, before pelleting the cells at 700 rpm for 7 minutes and discarding supernatant. Cells were resuspended slowly in 10 mL of fixative while vortexing gently. The suspension was centrifuged at 700 rpm for 7 minutes and the fixation procedure was repeated twice before cells were dropped onto Superfrost Poly+ slides (ThermoFisher Scientific) to let cells burst and chromosomes adhere to the surface. Slides were held with surfaces facing down towards water vapor for 5 seconds and then dried on a heating block, after which they were incubated with 1 mg/mL of pepsin in H_2O at 37 °C for 10 minutes. TelG-Cy3 PNA probe (Panagene, Daejeon, South Korea) was added 1:20 in hybridization buffer (consisting of 10 mM $NaHPO_4$ pH 6.4, 10 mM NaCl, 20 mM Tris pH 7.5, 70 % FA, Denhardt's solution, and 10 μL/mL ssDNA) together with 100 μg/mL cot1 DNA, hybridized at 80 °C for 3 minutes and subsequently incubated at rt for 2 hours. Slides were washed 3 times in 0.1 % Tween/PBS preheated to 55

°C and mounted in Vectashield Antifade Mounting Medium with DAPI. Cells were imaged at rt using a Leica DMRE microscope equipped with a 100x/1.25 N PLAN objective. Images were taken using the Hamamatsu C4880 camera and HiPic 32 software (Hamamatsu). Image brightness and contrast were adjusted using ImageJ.

Inhibition of MKL1 using CCG-1423

HL0 cells were incubated with indicated concentration of CCG-1423 for 24 or 48 hours at 37 °C and 5 % CO_2. The DMSO control used was equivalent to the highest amount of DMSO of the experiment, i.e. 10 or 20 µM condition. For *in vivo* administration, NSG mice were injected with HL0 cells by subcutaneous injection. After 6 days, 50 µl of 10 µM CCG-1423 or DMSO was injected intratumorally for 6 consecutive days. The volume of the tumor was calculated at the endpoint using a caliper.

Statistical analysis

Data are expressed as means +/- SD where indicated. Statistical analyses were performed using the GraphPad Prism 7 software (GraphPad Software, La Jolla, California, USA). Statistical significance between groups was assessed by 2-tailed Student *t*-test or one-way ANOVA with post-hoc Tukey test. Differences were considered significant when $P < 0.05$. For each figure, statistical analysis details are embedded in the figure legend.

References

1. Nagy N, Adori M, Rasul A, Heuts F, Salamon D, Ujvari D, et al. Soluble factors produced by activated CD4+ T cells modulate EBV latency. Proc Natl Acad Sci U S A. 2012 Jan 31;109(5):1512-7.

2. Shultz LD, Lyons BL, Burzenski LM, Gott B, Chen X, Chaleff S, et al. Human lymphoid and myeloid cell development in NOD/LtSz-scid IL2R gamma null mice engrafted with mobilized human hemopoietic stem cells. J Immunol. 2005 May 15;174(10):6477-89.

3. Marits P, Wikstrom AC, Popadic D, Winqvist O, Thunberg S. Evaluation of T and B lymphocyte function in clinical practice using a flow cytometry based proliferation assay. Clin Immunol. 2014 Aug;153(2):332-42.

4. Schindelin J, Arganda-Carreras I, Frise E, Kaynig V, Longair M, Pietzsch T, et al. Fiji: an open-source platform for biological-image analysis. Nat Methods. 2012 Jun 28;9(7):676-82.

5. Westerberg LS, Meelu P, Baptista M, Eston MA, Adamovich DA, Cotta-de-Almeida V, et al. Activating WASP mutations associated with X-linked neutropenia result in enhanced actin polymerization, altered cytoskeletal responses, and genomic instability in lymphocytes. J Exp Med. 2010 Jun 7;207(6):1145-52.

Table S1. Flow-cytometric assay of specific cell-mediated immune response in activated whole blood.*

Stimuli	Reference donor‡			Ctrl			C1			HL0			HL1			HL2		
	CD4+	CD8+	CD19+	CD4+	CD8+	CD19+	CD4+	CD8+	CD19+	CD4+	CD8+	CD19+	CD4+	CD8+	CD19+	CD4+	CD8+	CD19+
Medium	65	10	5	108	77	14	143	15	8	28	70	9	35	113	6	30	68	15
Phytohemagglutinin	93	34		602	598					171	370		119	189				
Pokeweed mitogen	10138	2653	886	16724	1496	2971	34620	1629	612	2421	8970	62	1256	5361	37	3092	7211	108
Concanavalin A	11882	6164		11467	5324		16127	3380		5847	7084		805	635		2007	6947	
Prevenar vaccine	520	42		794	95		109	51		70	108		32	55		16	73	
Tetanus toxin	85	20		83	27		17211	464		50	48		32	72		190	113	
Influenza A vaccine	1638	95		1540	237		1730	177		199	53		1079	328		103	93	
PPD	2149	165		665	131		7656	272		6988	452		2873	194		40	110	
Candida	6650	64		14077	238		8965	152		1504	103		1781	222		6477	218	
Staphylococcal enterotoxin A/B	34350	16542		52044	12633		53077	7461		14260	23689		3058	3250		8705	22103	
Varicella zoster virus	190	61		91	44		701	51		170	59		130	154		197	84	

*Numbers indicate proliferating lymphocytes as determined by increased size in forward scatter by flow cytometry. Whole blood was stimulated for 7 d in medium alone or supplemented with indicated stimuli. At d 7, numbers of $CD4^+$, $CD8^+$, and $CD19^+$ blast cells were determined. ‡Age-matched reference donor. The results should be interpreted in relation to infection and vaccination history.

Figure S1

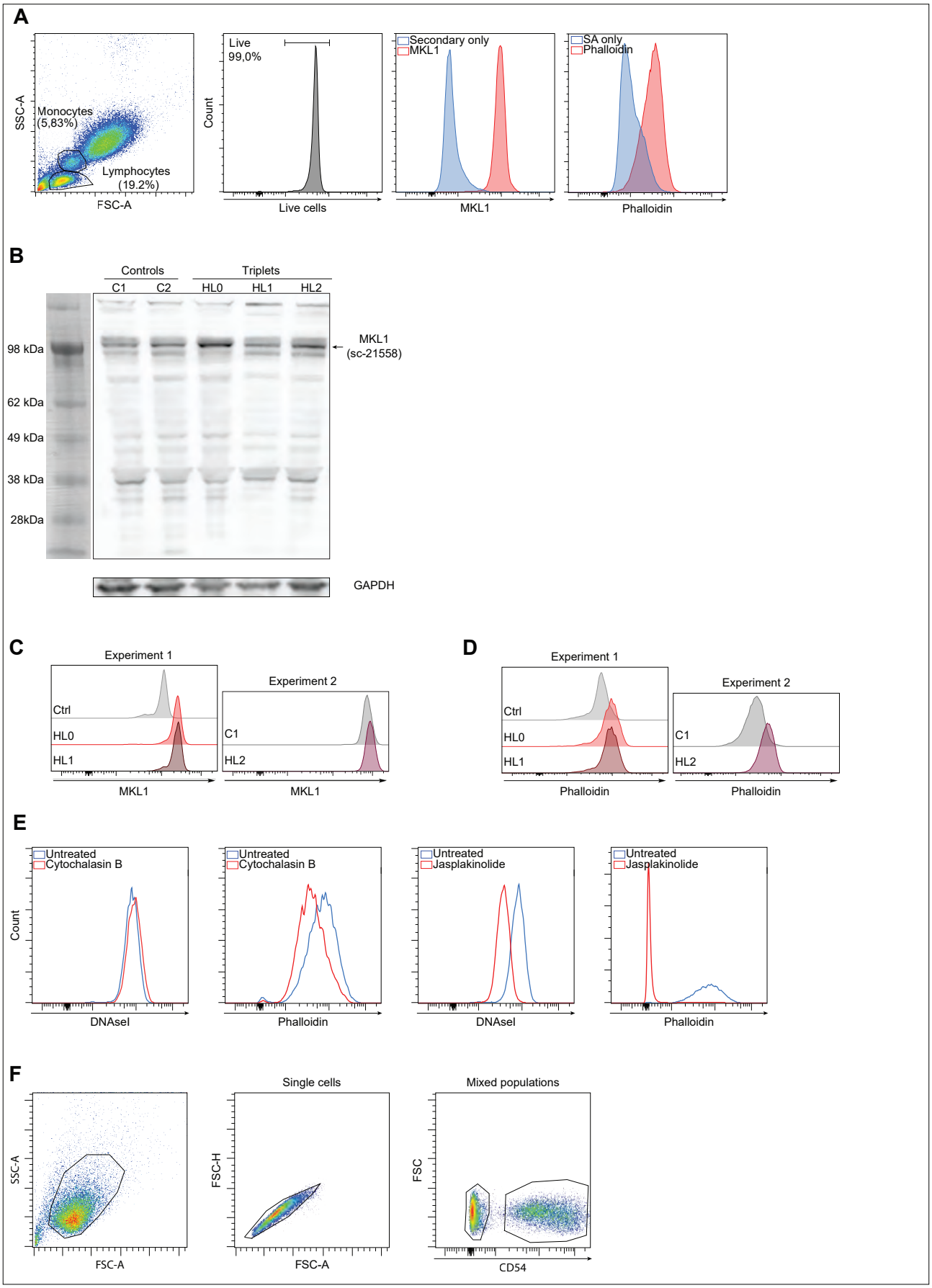
A
SSC-A
Monocytes
(5,83%)
Lymphocytes
(19.2%)
FSC-A
Live
99,0%
Count
Live cells
Secondary only
MKL1
MKL1
SA only
Phalloidin
Phalloidin
B
Controls
Triplets
C1
C2
HL0
HL1
HL2
98 kDa
62 kDa
49 kDa
38 kDa
28kDa
MKL1
(sc-21558)
GAPDH
C
Experiment 1
Experiment 2
Ctrl
HL0
HL1
C1
HL2
MKL1
MKL1
D
Experiment 1
Experiment 2
Ctrl
HL0
HL1
C1
HL2
Phalloidin
Phalloidin
E
Untreated
Cytochalasin B
Count
DNAseI
Untreated
Cytochalasin B
Phalloidin
Untreated
Jasplakinolide
DNAseI
Untreated
Jasplakinolide
Phalloidin
F
SSC-A
FSC-A
Single cells
FSC-H
FSC-A
Mixed populations
FSC
CD54

Figure S1. (A) FACS gating strategy for analysis of immune cells in PBMCs. Subpanels (left to right): gating of monocytes and lymphocytes using forward vs side scatter; gating on living cells using Aqua Dead Cell Stain; fluorescence intensity of goat Alexa568 conjugated anti-rabbit only (secondary; blue) and together with rabbit anti-human MKL1 (red); fluorescence intensity of streptavidin-APC/Cy7 only (SA; blue) and together with phalloidin-biotin (Ph; red). (B) Full Western Blot of LCLs from controls (C1 and C2) and triplets (HL0, HL1 and HL2) using the anti-human MKL1 antibodies sc-21558. (C) MKL1 expression in primary monocytes by flow cytometry. Subpanels represent experiments conducted at separate time points. (D) Phalloidin expression in primary monocytes by flow cytometry. Subpanels represent experiments conducted at separate time points. (E) Controls for detection of G-actin and F-actin using DNAseI and phalloidin staining, respectively. Flow cytometry analysis of G-actin and F actin content in LCLs from C2 treated or untreated for 30 min with 2 μM of cytochalasin B (CB; to depolymerize F-actin) or 0.5μM of jasplakinolide (Jas.; to stabilize F-actin). Note that cytochalasin B induced a small increase in DNAseI (labeling G-actin) and a decrease in Phalloidin (labeling F-actin, left panels). Jasplakinolide induced a decrease in DNAseI (right panels). Since jasplakinolide competes with phalloidin binding sites on F-actin, changes in F-actin content can't be visualized. (F) Gating strategy for analysis of F and G-actin content in LCLs. Subpanels (left to right): gating of LCLs using forward and side scatter; gating on single cells using FCS-Area vs FCS-Height; gating of the CD54-Alexa647 positive and negative populations.

Figure S2

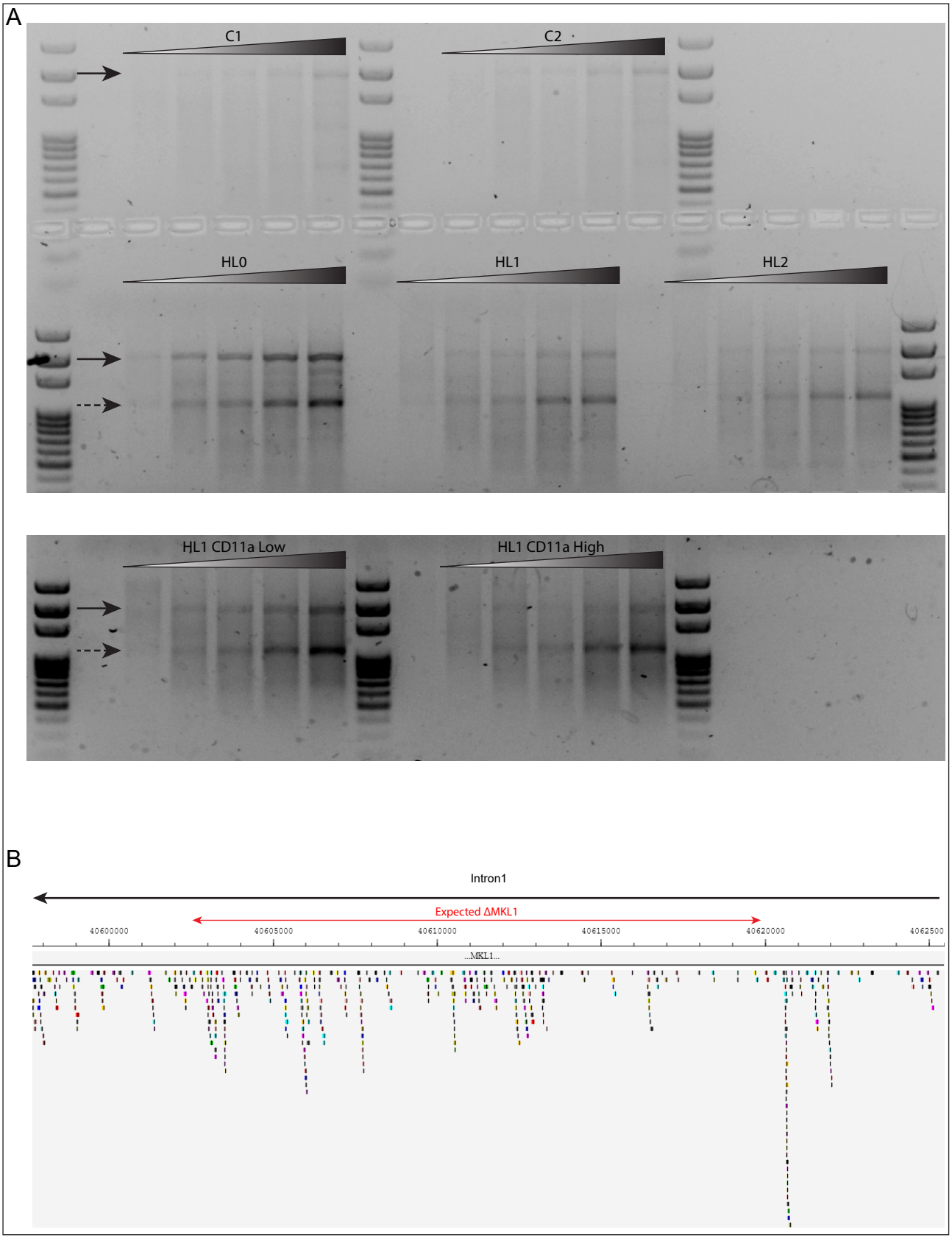
A
C1
C2
HL0
HL1
HL2
HL1 CD11a Low
HL1 CD11a High
B
Intron1
Expected ΔMKL1
40600000
40605000
40610000
40615000
40620000
4062500
...MKL1...

Figure S2. (A) PCR products using primer pair flanking the expected ΔMKL1. The PCR revealed a band present in all samples (upper band, plain arrow) and a band of lower molecular weight specific to the triplets indicating the intronic deletion (lower band, dashed arrow). The genomic DNA from each sample was subjected to 20, 25, 30, 35, 40 or 42 PCR cycles as seen on the gel from left to right. Upper image, top row: healthy donors C1 and C2; bottom row: triplets HL0, HL1 and HL2; Bottom image HL1 cells after been sorted for CD11a low and CD11a high populations. (B) Schematic of MKL1 first intron showing the transcription factors sites in the expected ΔMKL1 and flanking regions (modified from Gene Transcription Regulation Database, http://gtrd.biouml.org/).

Figure S3

A

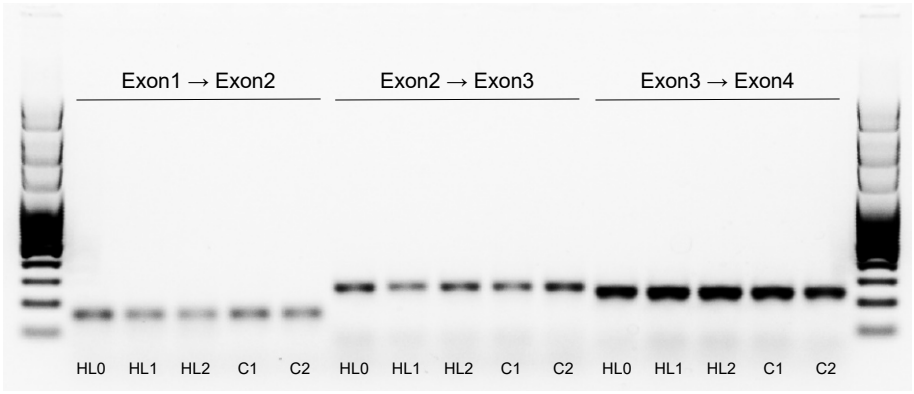
Exon1 → Exon2
Exon2 → Exon3
Exon3 → Exon4
HL0 HL1 HL2 C1 C2 HL0 HL1 HL2 C1 C2 HL0 HL1 HL2 C1 C2

B

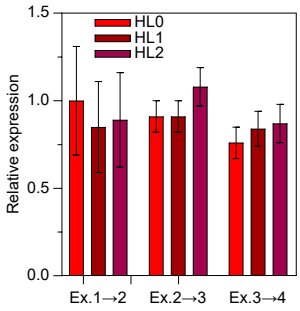
HL0
HL1
HL2
Relative expression
1.5
1.0
0.5
0.0
Ex.1→2
Ex.2→3
Ex.3→4

Figure S3. Detection of exon boundaries between exons 1 and 2, 2 and 3, 3 and 4, 4 and 5 and 5 and 6 in controls C1 and C2 and in triplets HL0, HL1 and HL2. (A) Exon boundaries were amplified y PCR and run on agarose gel. (B) Exon boundaries were detected by RT-qPCR. Results were normalized to C1 and C2 mean value.

Figure S4

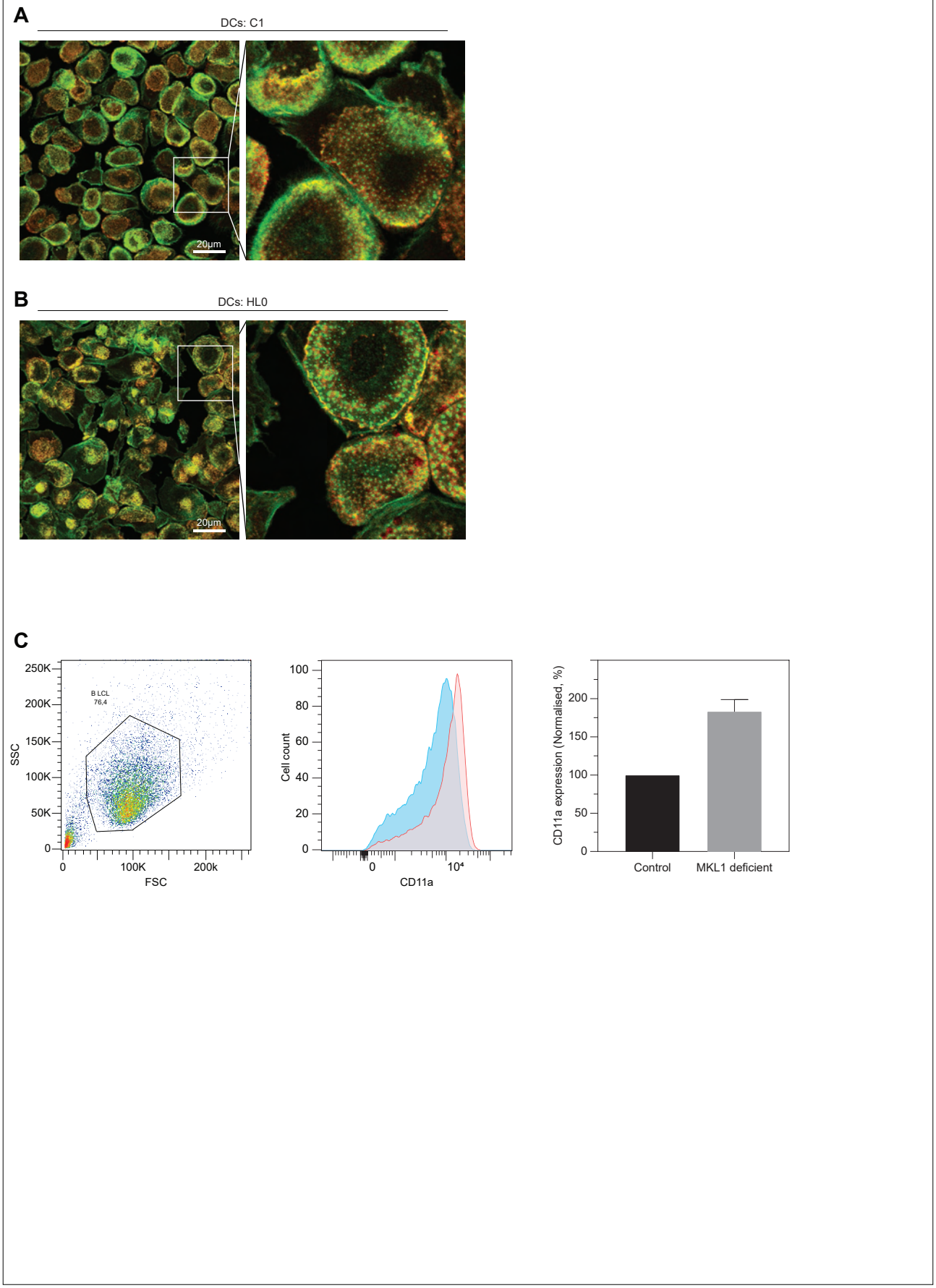
A
DCs: C1
20µm
B
DCs: HL0
20µm
C
B LCL
76.4
SSC
FSC
250K
200K
150K
100K
50K
0
100K
200k
Cell count
CD11a
10⁴
CD11a expression (Normalised, %)
Control
MKL1 deficient

Figure S4. (A) and (B) Representative images of monocytes derived dendritic cells from C2 control and triplet HL0, respectively . Cells were stained with AlexaFluor-488 tagged Phalloidin (green) together with a mouse anti-vinculin antibody followed by an anti-mouse AlexaFluor-568 antibody (red). Cells were images using Leica SP5 confocal microscope equipped with an HCX PL APO CS 63.0x N.A. 1.40 Oil UV objective. Original magnification: x630. (C) CD11a expression levels on control (blue histogram) and MKL1 deficient (red histogram) B LCLs. First graph, gating of the LCLs; second graph, CD11a expression (histograms); third graph, quantification of CD11a expression.

Figure S5

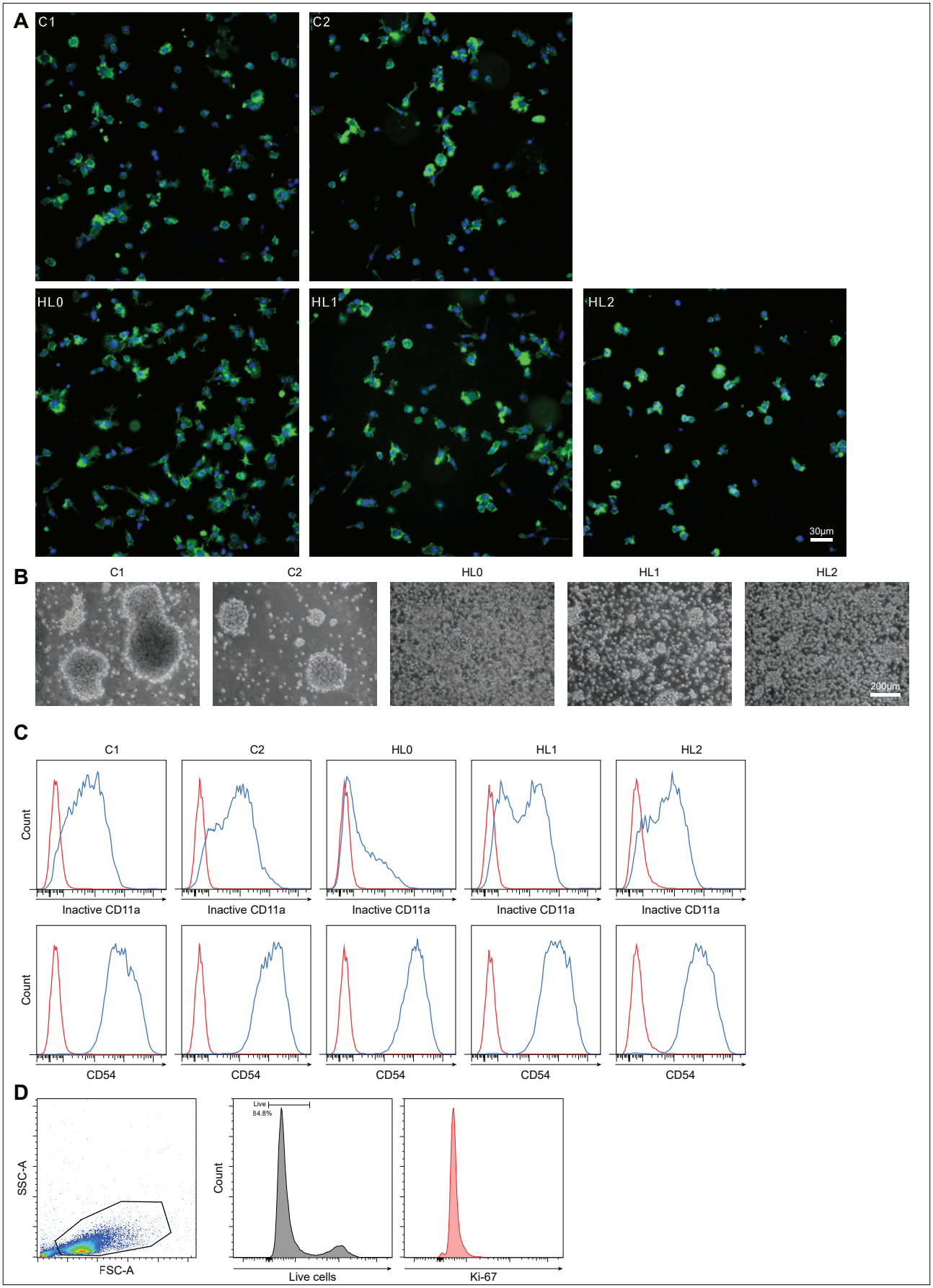
A
C1
C2
HL0
HL1
HL2
30μm
B
C1
C2
HL0
HL1
HL2
200μm
C
C1
C2
HL0
HL1
HL2
Count
Inactive CD11a
CD54
D
SSC-A
FSC-A
Live
84.8%
Count
Live cells
Ki-67

Figures S5. (A) Representative immunocytochemistry images of B cells adhering to glass slides coated with fibronectin and anti-CD19. Microscope: Leica DMRE; objective: 25x/0.75 PL-FL. Cells stained with phalloidin-Alexa488 (green) and mounted in Vectashield Antifade Mounting Medium with DAPI (blue). Images taken at room temperature using the Hamamatsu C4880 camera and LAS AF acquisition software; brightness and contrast adjusted using ImageJ. Original magnification: 250X. (B) Representatives images of LCLs aggregates after 24hs in culture at 37oC. Images taken at room temperature using a Motic AE30 microscope equipped with 10x/0.25 Plan Achromat Phase lens and a Moticam 580. Original magnification: 100X. (C) Surface expression of inactive CD11 and CD54 in the controls and triplets LCLs. (D) FACS gating strategy for cultured B cells. Subpanels (left to right): gating of B cells using forward vs side scatter; live/dead staining using AmCyan; fluorescence intensity of Ki67-APC.

Figure S6

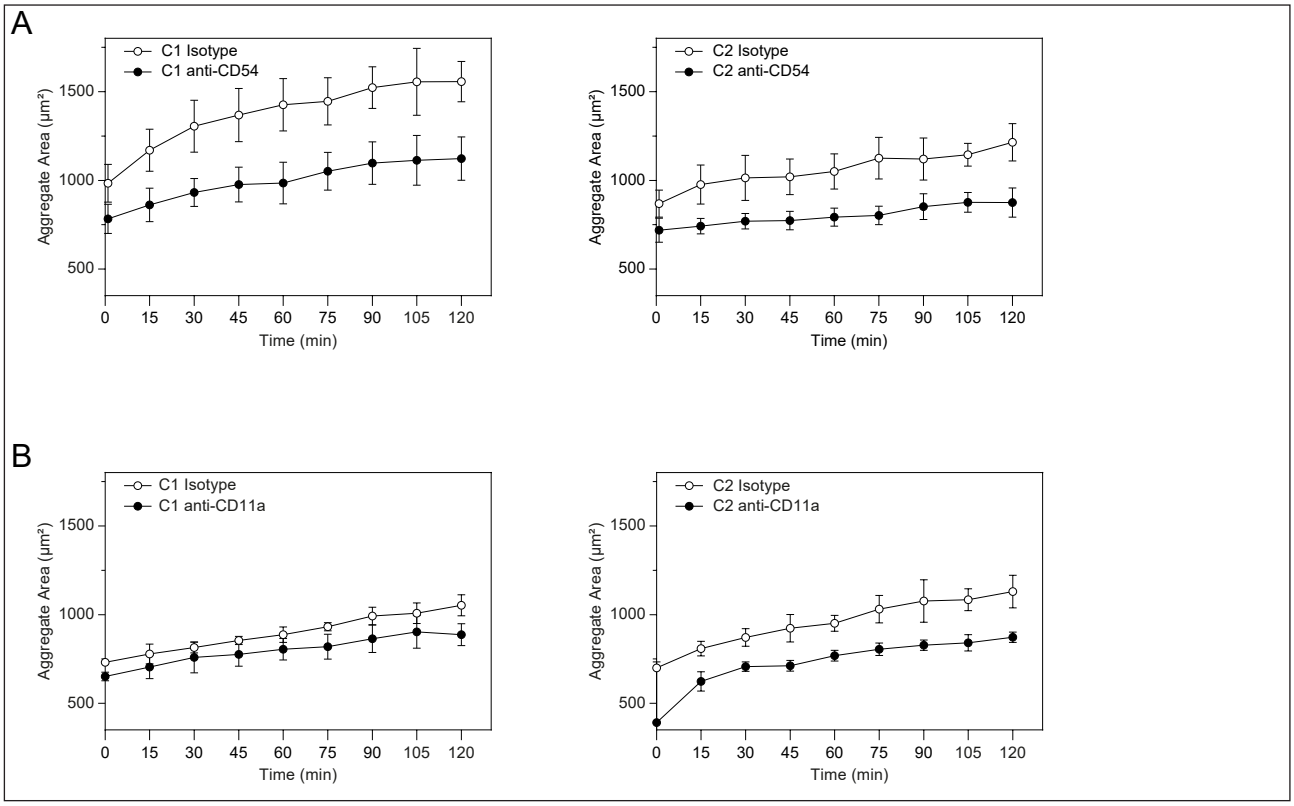
A
C1 Isotype
C1 anti-CD54
C2 Isotype
C2 anti-CD54
B
C1 Isotype
C1 anti-CD11a
C2 Isotype
C2 anti-CD11a
Aggregate Area (µm²)
Time (min)
500
1000
1500
0
15
30
45
60
75
90
105
120

Figure S6. Aggregation of C1 and C2 cell was monitored over 2 hours by time lapse microscopy in presence of blocking antibodies directed against CD54 and CD11a or in presence of isotype control antibody. (A) Average area of C1 and C2 cells aggregates in presence of 10µg/ml of anti-CD54 antibody or (B) anti-CD11a antibody.

Figure S7

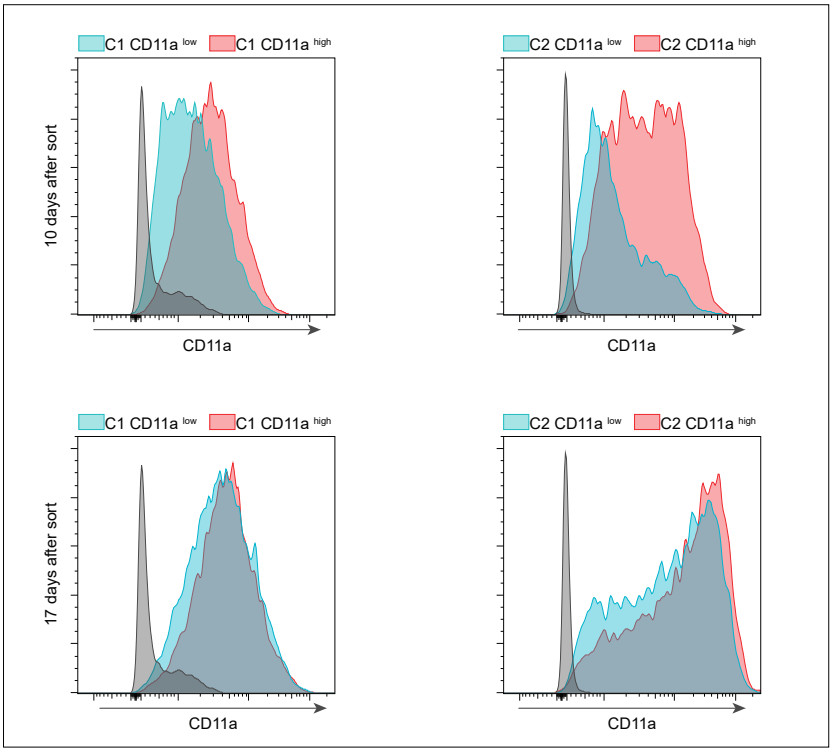
C1 CD11a low
C1 CD11a high
C2 CD11a low
C2 CD11a high
10 days after sort
17 days after sort
CD11a

Figure S7. CD11a expression in C1 and C2 cells sorted for CD11a low and high expression. Expression of CD11a was assessed by flow cytometry 10 and 17 days after sort.

Figure S8

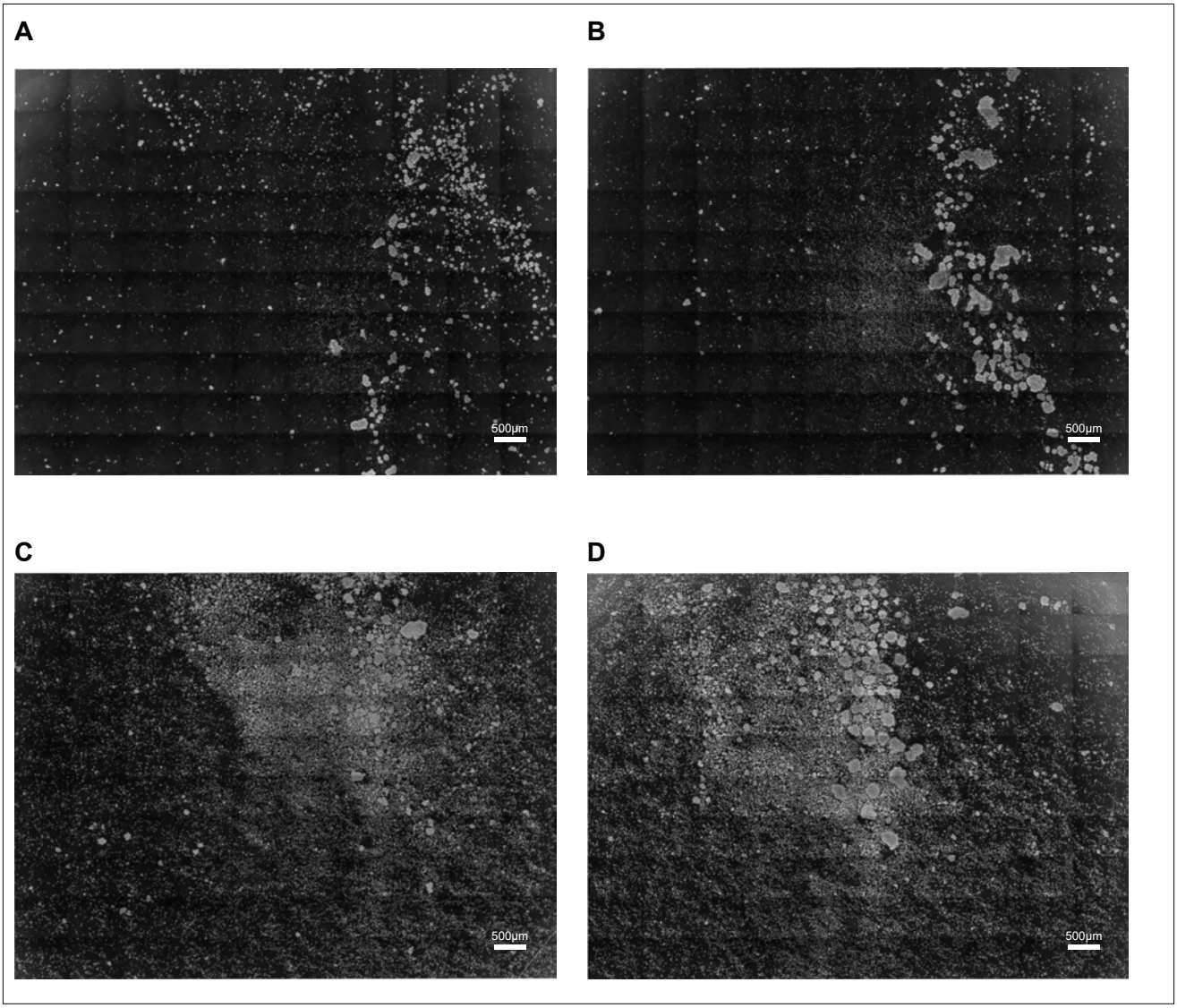

Figure S8. Aggregation of C1 and C2 sorted for CD11a low and high expression. On day 16, 200 000 cells of (A) C1 CD11a^{low}, (B) C1 CD11a^{high}, (C) C2 CD11a^{low} and (D) C2 CD11a^{high} were plated in a 24 wells plate and left at 37^{o}C for 24 hours before being imaged using a 10x objective. Image composed of 100 images stitched together.

Figure S9

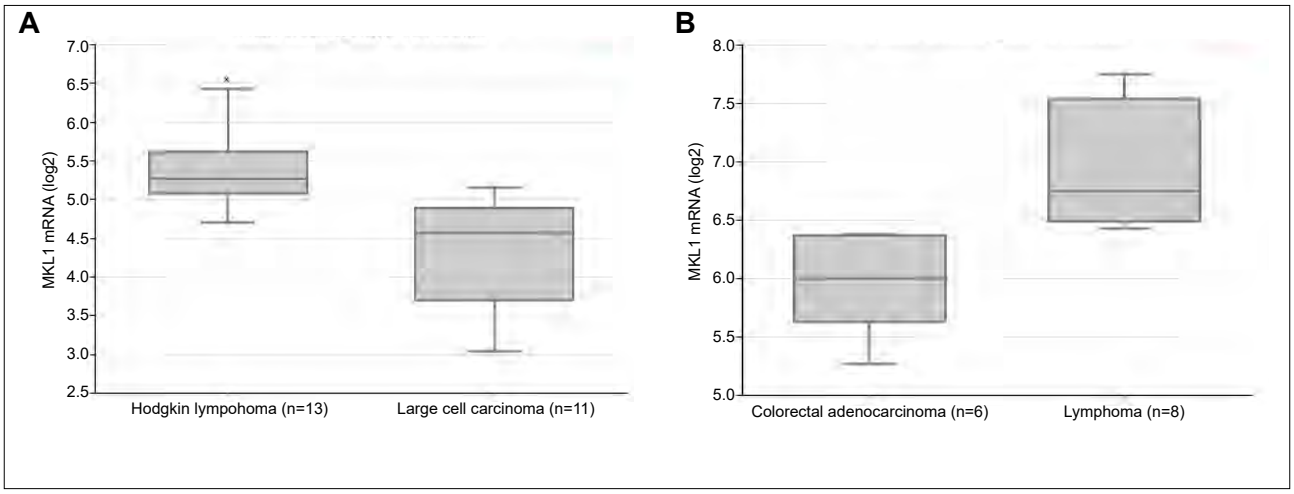
A
MKL1 mRNA (log2)
7.0
6.5
6.0
5.5
5.0
4.5
4.0
3.5
3.0
2.5
Hodgkin lympohoma (n=13)
Large cell carcinoma (n=11)
B
MKL1 mRNA (log2)
8.0
7.5
7.0
6.5
6.0
5.5
5.0
Colorectal adenocarcinoma (n=6)
Lymphoma (n=8)

Figure S9. Expression of MKL1 in (A) HL and carcinoma and (B) in lymphoma and colorectal adenocarcinoma patients from the R2 database (R2: Genomics Analysis and Visualization Platform; http://r2.amc.nl).